From activation to stabilization

Different applications of a frustrated Lewis pair

Boom, D.H.A.

Chapter 2

Catalytic Dehydrogenation of Amine-Boranes using Geminal Phosphino-Boranes

Abstract: The reaction of FLP *t*Bu$_2$PCH$_2$BPh$_2$ with the amine-boranes NH$_3$·BH$_3$ and Me$_2$NH·BH$_3$ leads to the formation of the corresponding FLP-H$_2$ adducts as well as novel 5-membered heterocycles that result from capturing of the in situ formed amino-borane by a second equivalent of FLP. The sterically more demanding *t*Bu$_2$PCH$_2$BMes$_2$ does not form such a 5-membered heterocycle when reacted with Me$_2$N·BH$_3$ and its H$_2$ adduct liberates dihydrogen at elevated temperatures, promoting the metal-free catalytic dehydrogenation of amine-boranes. Targeting increased reactivity, our rational catalyst design revealed that Mes$_2$PCH$_2$B*t*Bu$_2$ is a highly interesting and potential catalyst for this reaction.

Manuscript: In preparation

2.1 Introduction

During the past decades tremendous breakthroughs were made in main-group mediated chemical transformations and new strategies for single bond activations were discovered. Especially since the discovery of frustrated Lewis pairs (FLPs) in 2006 to heterolytically cleave dihydrogen[1] a new research field emerged for metal-free stoichiometric and catalytic chemical transformations, such as hydrogenation and dehydrogenation reactions.[2]

As a substrate for catalytic dehydrogenation, amine-boranes gained a lot of attention due to their potential application as dihydrogen storage material;[3] in particular ammonia-borane (AB) is of interest as is contains a high weight percentage of dihydrogen (19.6%).[4] Furthermore, the products resulting of amine-borane dehydrogenation are valuable, with many potential applications in material science.[5] To date, a lot of research has been conducted on the catalytic dehydrogenation of amine-boranes by transition metal (TM) complexes.[6] Alternatively, efforts have been made in the development of group 1 and 2 catalysts,[7] and recently frustrated Lewis pairs have been reported as efficient TM-free catalysts for amine-borane dehydrogenation.

The first FLP catalyst for ammonia-borane dehydrogenation was reported by Stephan and Erker (**I**, Figure **1**) utilizing a transfer hydrogenation step for catalyst regeneration.[8] After this, our group in collaboration with Uhl and co-workers reported on the catalytic dehydrogenation of dimethylamine-borane (DMAB) by phosphino-alane **II**.[9] In 2016, Rivard and co-workers extended the field and showed that iminoborane **IV** can dehydrogenate methylamine-borane (MAB) at 70 °C, utilizing 2 mol% of **IV**.[10] In the same year, Aldridge et al. reported that the xanthene-based phosphino-borane **V** is capable of dehydrogenating AB, MAB and DMAB with catalysts loadings down to 1 mol%.[11] Recently Uhl and co-workers found that the gallium analogue of **II**, phosphino-galane **III**, can be applied for ammonia- and dimethylamine-borane dehydrogenation too.[12] At the same time, the group of Bourissou showed that phosphino-borane **VI** rapidly converts a variety of amine-borane substrates to the corresponding dehydrogenated products.[13]

We developed geminal phosphino-borane FLP **VII** (R = *t*Bu, R' = Ph; **1**) bearing a methylene linker, which shows reactivity towards a variety of small molecules and metal complexes.[14,15] Herein, we describe the (catalytic) dehydrogenation of amine-boranes by

such geminal frustrated Lewis pairs, including a rational catalyst design approach targeting increased reactivity.

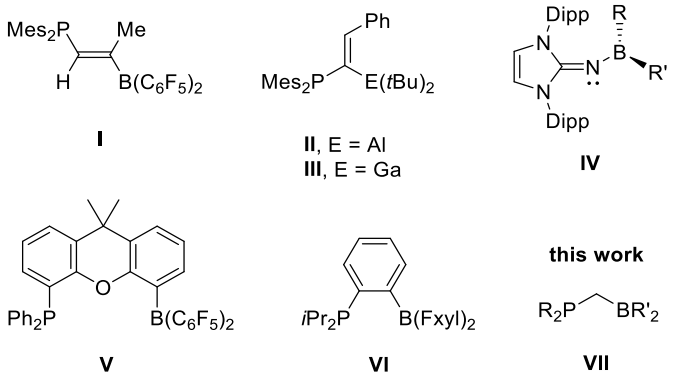

Figure 1. FLP catalysts for amine-borane dehydrogenation.

2.2 Results and Discussion

Treatment of 2 equivalents of tBu$_2$PCH$_2$BPh$_2$ (**1**) with 1 equiv of ammonia-borane ($H_3N{\cdot}BH_3$, AB) in THF at room temperature resulted in immediate consumption of AB, along with formation of dihydrogen adduct **2** (δ $^{31}P\{^1H\} = 59.0$ ppm) and 5-membered heterocycle **3** (δ $^{31}P\{^1H\} = 56.7$ ppm) in a 1:1 ratio. The products can be separated by extraction of **3** into *n*-pentane (leaving pure **2** as residue in 57% yield) and subsequent filtration of the combined extracts over alumina to remove trace amounts of **2** from the extract, giving **3** as white solid in 74% yield. H_2 adduct **2** displays a double multiplet in the ^{31}P NMR spectrum with a $^1J_{P,H}$ coupling of 453.2 Hz, and a doublet in the ^{11}B NMR spectrum ($^1J_{B,H}$ = 83.5 Hz), which is characteristic for a P–H and B–H bond, respectively. Single crystals suitable for X-ray diffraction analysis of **2** were obtained from *n*-pentane at 4 °C, which confirmed the formation of the FLP-H_2 adduct that was previously obtained from the reaction of **1** with dihydrogen.[14a] In the solid state, the boron center in **2** is strongly pyramidalyzed (Σ(CB1C) 330.5°), which also resembles the upfield ^{11}B NMR shift (δ $^{11}B\{^1H\} = -10.1$ ppm). In contrast to the *o*-phenylene-bridged P/B FLP-H_2 adduct reported by Bourissou and co-workers,[13] dihydrogen adduct **2** is stable at room temperature in the

solid state and in solution, and only slowly released dihydrogen when kept at elevated temperatures for a long time (2 hours at 80 °C).[16]

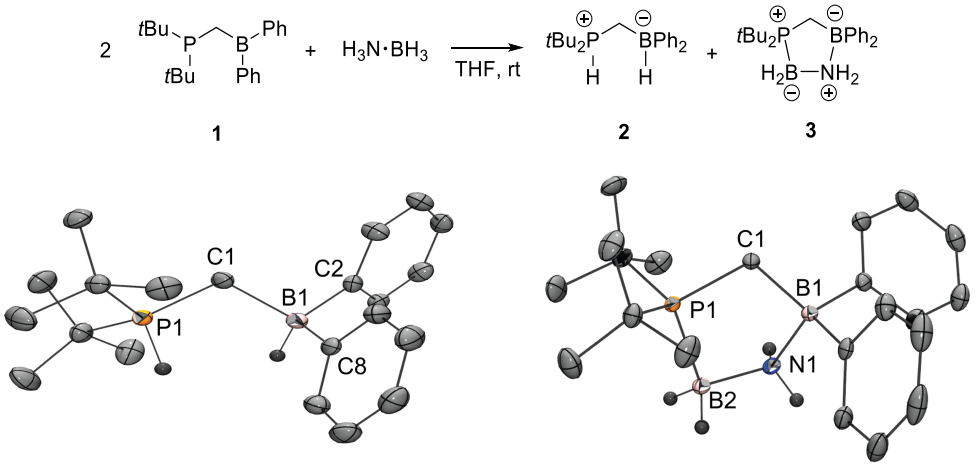

Scheme 1. Reaction of 2 equivalents of FLP **1** with 1 equiv of ammonia-borane (top) and the molecular structures (bottom) of **2** (left) and **3** (right) (ellipsoids at 50% probability, FLP-hydrogens, and a toluene molecule for **2** are omitted for clarity). Selected bond lengths (Å) and angles (°) for **2**: P1−C1 1.7759(16), B1−C1 1.683(2), P1−C1−B1 113.48(11), Σ(CB1C) 330.5 **3**: P1−C1 1.8155(10), C1−B1 1.6626(14), B1−N1 1.6321(13), N1−B2 1.5898(14), B2−P1 1.9606(11).

The formation of the 5-membered heterocycle **3** is believed to be the result of trapping of the highly polarized amino-borane intermediate $H_2N{=}BH_2$ by the second equivalent of FLP **1**. In the $^{11}B\{^1H\}$ NMR spectrum, **3** displays a singlet resonance ($\delta = -1.95$ ppm) for the FLP's boron moiety together with a characteristic doublet ($\delta = -20.7$ ppm, $^1J_{B,P} = 85.5$ Hz) that can be ascribed to the amino-borane fragment. The corresponding $^{31}P\{^1H\}$ NMR spectrum supports this notion as a broad signal was observed at $\delta = 56.7$ ppm, which is common for such B–P interactions.[17] X-ray diffraction analysis of suitable single crystals of **3**, obtained by layering a solution of **3** in DCM with pentane, unambiguously established the formation of the P-C-B-N-B based 5-membered heterocycle (Scheme 1, bottom right). Compared to the previously reported Al- and Ga-based 5-membered heterocycles formed by $H_2N{=}BH_2$ trapping using the corresponding FLPs,[9,12] **3** contains a shorter P1–B2 bond

(1.9606(11) Å), as well as a shorter E1–N1 bond (E = B for **3**) (1.6321(13) Å), suggesting that the trapped $H_2N{=}BH_2$ fragment is more tightly bound to the FLP in **3**.

In order to gain more insight into the mechanism of this dehydrogenation reaction, FLP **1** was reacted with the deuterated analogue of AB, $NH_3{\cdot}BD_3$, which resulted in selective N–H to P and B–D to B transfer according to ^{31}P and ^{11}B NMR spectroscopy. This suggests a similar double hydrogen transfer mechanism being operative as was observed previously by Manners *et al*. for dihydrogen transfer from ammonia-borane to sterically encumbered amino-boranes.[18] Analysis of the formation of **2** by density functional theory (DFT) calculations at the *ω*B97X–D/6-311G** level of theory revealed that the interaction of ammonia-borane with FLP **1** leads to the formation of a three-center-two-electron adduct **4** as intermediate (Figure **2**), which enables dihydrogen transfer from $NH_3{\cdot}BH_3$ in a concerted manner via a 7-membered transition state forming phosphonium-borate **2** and one equivalent of amino-borane $H_2N{=}BH_2$. The overall process is exergonic, and the low barrier ($\Delta G^{\ddagger}$ = 13.1 kcal/mol, $\Delta E^{\ddagger}$ = 3.34 kcal/mol) for $\mathbf{TS_{4\text{-}2}}$ is in good agreement with the experimentally observed facile reaction (instantaneous at 0 °C). Additionally, trapping of the amino-borane $H_2N{=}BH_2$ fragment by a second equivalent of FLP **1** makes the overall reaction even more exergonic ($\Delta G_{\mathbf{trapping}}$ = –17.5 kcal/mol, $\Delta E_{\mathbf{trapping}}$ = –34.7 kcal/mol).

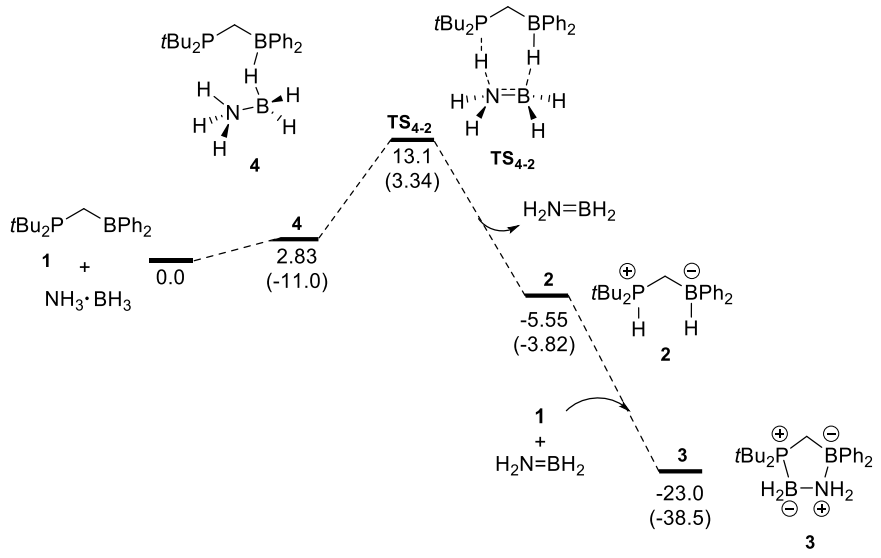

Figure 2. Gibbs free energy and (energy) profile calculated for dehydrogenation of ammonia-borane by FLP **1**.

Under the same conditions, the reaction of 2 equiv of **1** with the bulkier dimethylamine-borane ($Me_2NH{\cdot}BH_3$, DMAB) resulted in rapid formation of the known FLP-H_2 adduct **2** together with the methylated analogue of **3**, compound **5** (Scheme **2**). $^{31}P\{^1H\}$ NMR spectroscopy of the reaction mixture revealed comparable resonance signals as for the reaction of **1** with AB (δ $^{31}P\{^1H\}$ = 59.0 ppm for the FLP-H_2 adduct, and a broad resonance signal for the methylated heterocycle; δ $^{31}P\{^1H\}$ = 43.0 ppm). In contrast to **3**, the $^1J_{B,P}$ coupling in **5** is significantly smaller and no clear doublet was observed in the $^{11}B\{^1H\}$ NMR spectrum. DFT calculations at the ωB97X–D/6-311G** level of theory suggest that the same mechanism takes place. With an overall barrier (ΔG) of only 14.1 kcal/mol ($\Delta E^{\ddagger}$ = 4.37 kcal/mol), the experimentally observed reaction rate is in good agreement with the DFT calculations. Interestingly, when a sample of the reaction mixture was kept for a prolonged period at room temperature signals of the dimeric $(Me_2NBH_2)_2$ started to appear in the $^{11}B\{^1H\}$ NMR spectrum due to release of the $Me_2N{=}BH_2$ fragment from **5** and subsequent dimerisation. This indicates that increasing the steric bulk of the substrate reduces the bond strength of the amino-borane fragment to FLP **1**, which suggests that increasing the steric bulk of the FLP's substituents should also prevent adduct formation.

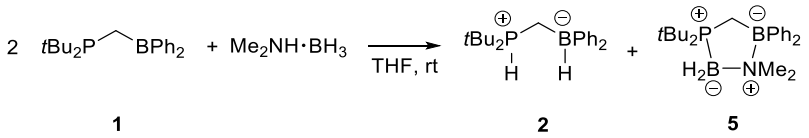

Scheme 2. Reaction of 2 equivalents of FLP **1** with dimethylamine-borane.

Encouraged by these findings, we set out to design a FLP system that disfavors amino-borane adduct formation. Interestingly, DFT calculations at the ωB97X–D/6-31G* level of theory showed that only a slight change of the system could already prevent adduct formation. FLP tBu$_2$PCH$_2$BMes$_2$ (**6**) bearing the bulkier mesityl substituents on boron was found to disfavor adduct formation with $Me_2N{=}BH_2$ (ΔG = 15.3 kcal/mol), which makes **6** an interesting synthetic target for catalytic dehydrogenation. Following the same synthetic strategy used for our previously reported FLP **1**,[14a] the reaction of tBu$_2$PCH$_2$Li with 1

equivalent of $ClBMes_2$ cleanly afforded **6** that after work up was isolated as an orange solid in 99% yield. The $^{31}P\{^1H\}$ and $^{11}B\{^1H\}$ NMR resonances of **6** are rather similar compared to **1**, namely a sharp singlet at 26.9 ppm and a broad singlet at 82.5 ppm, respectively. X-ray diffraction analysis of orange crystals obtained by cooling a saturated heptane solution of **6** to –20 °C showed that the boron empty p-orbital is rotated away from the phosphorus lone-pair (torsion angle P1–C1–B1–C11 = 168.9°) and that the boron center bears a planar geometry (∑(CB1C) = 359.8°), making any LA···LB type of interaction negligible (Scheme **3**). Interesting to note is the physical appearance of FLP **6**; whereas phenyl-substituted FLP **1** is an oil at room temperature, the mesityl-substituted analogue **6** is a solid, which facilitates the handling of the compound.

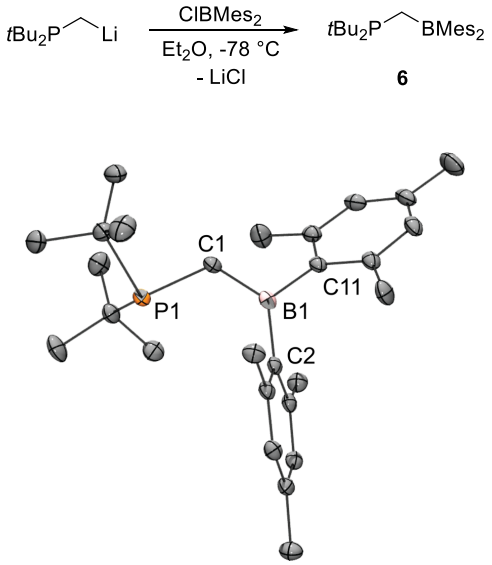

Scheme 3. Synthesis of FLP **6** (top) and the molecular structure (bottom; ellipsoids at 50% probability, hydrogen atoms are omitted for clarity). Selected bond lengths (Å) and angles (°) for **6**: P1−C1 1.8605(17), C1−B1 1.582(3), P1−C1−B1 124.21(12), P1−C1−B1−C11 168.9(12), Σ(CB1C) 259.8.

Under similar conditions, FLP **6** (2 equiv) was reacted with 1 equiv of ammonia-borane in 2-MeTHF (2-methyltetrahydrofuran) at room temperature. After approximately 1 hour at room temperature, the $^{11}B\{^1H\}$ and $^{31}P\{^1H\}$ NMR spectra of the reaction mixture revealed

that **6** was fully converted into FLP-H_2 adduct **7** (δ $^{31}P\{^1H\}$ = 56.5 (s); $^{11}B\{^1H\}$ = –15.0 (s)) and the 5-membered heterocycle **8** (δ $^{31}P\{^1H\}$ = 58.1 (br. s); $^{11}B\{^1H\}$ = 1.95 (s), –23.2, (s)), along with the formation of traces of dehydrogenation products such as borazine, cyclotriborazane (CTB) and *B*-(cyclodiborazanyl)aminoborohydride (BCDB) and a few unidentified products (Scheme **4**).

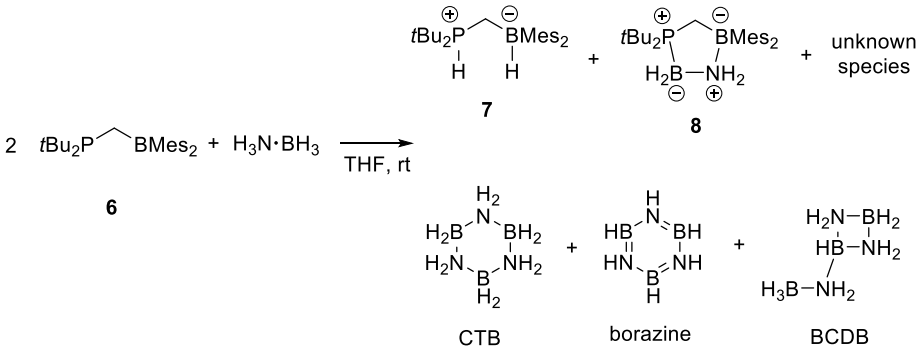

Scheme 4. The reaction of 2 equivalents of **6** with dimethylamine-borane.

Interestingly, heating the reaction mixture to 70 °C led to almost complete disappearance of H_2-adduct **7** and heterocycle **8**, concomitant with an increase of dehydrogenation products together with the formation of degradation products, such as $Mes_2B{=}NH_2$ (δ $^{11}B\{^1H\}$ = 44.1 (br. s))[19] and tBu$_2$PCH$_3$·BH$_3$ (δ $^{31}P\{^1H\}$ = 39.9 (m); $^{11}B\{^1H\}$ = –40.8 (d, $^1J_{B,P}$ = 57.8 Hz)), as was observed by $^{11}B\{^1H\}$ and $^{31}P\{^1H\}$ NMR spectroscopy (Figure **3**). In addition, also regeneration of FLP **6** was observed, suggesting that **6** could play a role in the catalytic amine-borane dehydrogenation, which is interesting since only a few FLPs are reported to catalyze the dehydrogenation of AB.[11,12,13]

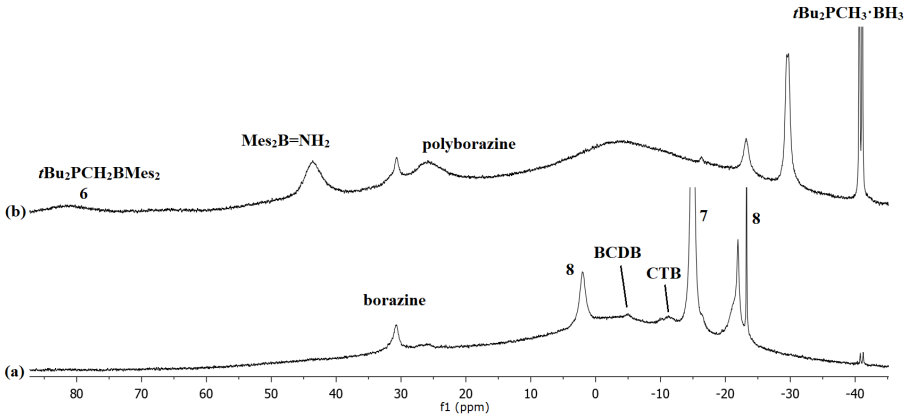

Figure 3. $^{11}B\{^1H\}$ NMR spectra of ammonia-borane and **6** mixed in a 1:2 ratio after (a) 1h at room temperature in 2-MeTHF, (b) the reaction mixture after heating to 70 °C overnight.

The labile character of both the FLP-H_2 adduct **7** and the 5-membered heterocycle **8** inspired us to investigate the possibility to apply **6** as a catalyst for ammonia-borane dehydrogenation. When 4 mol% of **6** was added to a suspension of $NH_3{\cdot}BH_3$ in 2-MeTHF, **6** was directly converted to H_2-adduct **7** and heterocycle **8** according to $^{11}B\{^1H\}$ and $^{31}P\{^1H\}$ NMR spectroscopy. Interestingly, when the reaction mixture was heated to 70 °C, a modest evolution of dihydrogen gas was visually observed as bubbles appeared from the reaction mixture. After 20 minutes at 70 °C, a mixture of dehydrogenation products was formed, yet the H_2-adduct **7** was still observable in both the $^{11}B\{^1H\}$ and $^{31}P\{^1H\}$ NMR spectrum, suggesting that this H_2-adduct is the resting state of the catalytic cycle (see experimental details). Prolonging the reaction time to 2 hours at 70 °C resulted in an increase of dehydrogenation B–N products and full degradation of the catalyst to tBu$_2$PCH$_3{\cdot}$BH$_3$ and $Mes_2B{=}NH_2$, and neither free FLP **6**, nor the dihydrogen adduct **7** were observed by NMR spectroscopy.

DFT calculations at the ωB97X–D/6-311G** level of theory confirm that dihydrogen adduct **7** is a plausible resting state in the catalytic dehydrogenation of AB. Similar to **1**, the calculations suggest that the initial interaction via a three-center-two-electron adduct is followed by a concerted double hydrogen abstraction step ($\Delta G^{\ddagger}$ = 25.1 kcal/mol, $\Delta E^{\ddagger}$ = 10.3 kcal/mol). This reaction step forming H_2-adduct **7** and $H_2N{=}BH_2$ was found to be exergonic

by 6.13 kcal/mol (ΔG) and 6.43 kcal/mol (ΔE). The energy barrier for dihydrogen release from **7** is the rate-determining step ($\Delta G^{\ddagger}$ = 27.3 kcal/mol, $\Delta E^{\ddagger}$ = 25.8 kcal/mol), which explains why H_2-adduct **7** can be observed by NMR spectroscopy during the reaction and why release of dihydrogen is observed after the reaction mixture is heated to elevated temperatures.

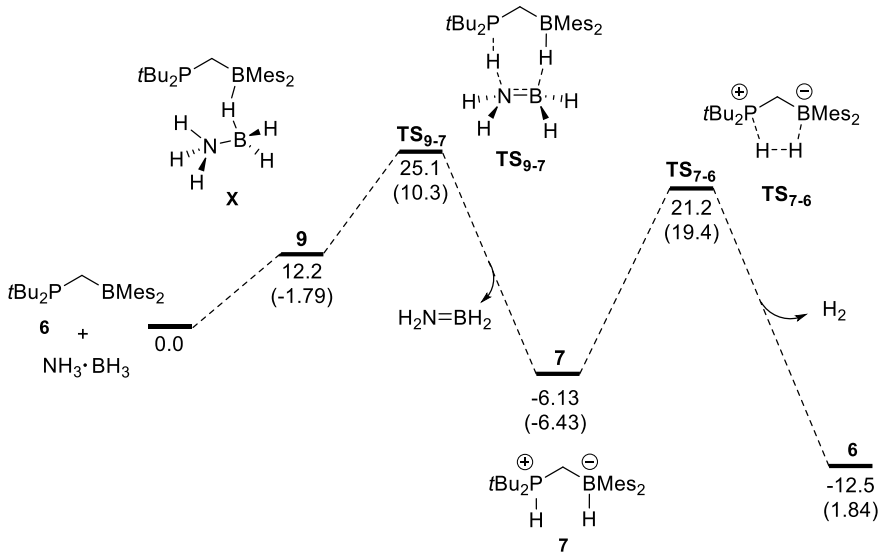

Figure 4. Gibbs free energy and (energy) profile calculated for AB dehydrogenation by **6**.

After having established the potential of FLP **6** as catalyst for amine-borane dehydrogenation, a solvent screening was performed. 2-Methyltetrahydrofuran was chosen as standard solvent for this catalytic dehydrogenation reaction, since it allows relatively high reaction temperatures (compared to DCM, Et_2O and THF) and the observed rate of the reaction was higher than when using toluene as solvent.[20] DME would also fit this requirement, however, at elevated temperatures degradation of **6** was found to be much faster in DME.

Under our standard catalytic conditions (4 mol% of **6**, 70 °C, 2.1 M DMAB, in 2-MeTHF) dimethylamine-borane was set for dehydrogenation. Initial formation of the FLP-H_2 adduct **7** was observed by $^{31}P\{^{1}H\}$ NMR spectroscopy, while upon heating to 70 °C this

species disappeared and the formation of dimeric $(NMe_2BH_2)_2$ was observed in the ^{11}B NMR spectrum, along with traces of other dehydrogenation products as well as the evolution of dihydrogen gas. Prolonging the reaction time resulted in an increase of $(NMe_2BH_2)_2$ formation which was monitored by ^{11}B NMR spectroscopy utilizing a sealed capillary filled with $B(OMe)_3$ as internal standard (Figure **5**). Over time, FLP **6** continuously consumed the $Me_2NH{\cdot}BH_3$ substrate, while producing the amino-borane dimer. Concomitant to the catalytic dehydrogenation, slow decomposition of the FLP catalyst **6** to tBu$_2$PCH$_3{\cdot}$BH$_3$ and several other unknown degradation products was observed. Eventually after 6 days at 70 °C, **6** was completely degraded and the production of $(NMe_2BH_2)_2$ stopped. Important to note is that in the absence of FLP **6**, no dehydrogenation was observed under the same reaction conditions.

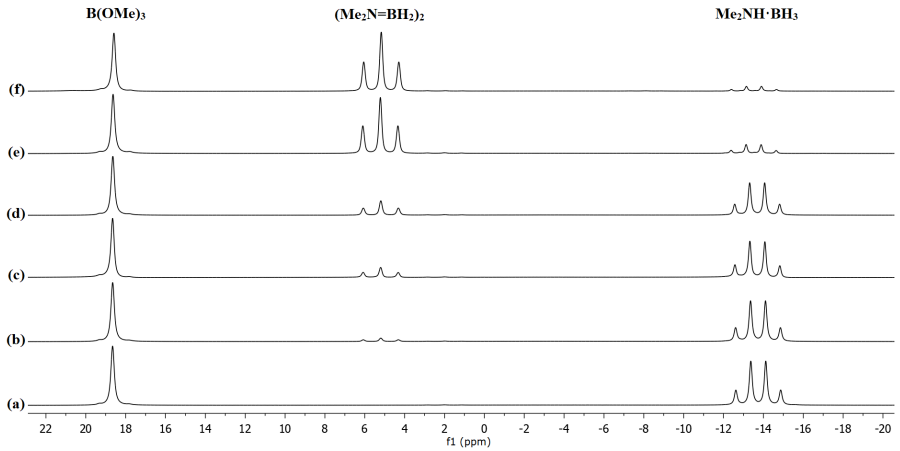

Figure 5. ^{11}B NMR spectra of catalytic dehydrogenation of $Me_2NH{\cdot}BH_3$ with 4% **6** in 2-MeTHF at 70 °C (a) direct after mixing, (b) after 50 min, (c), after 2.5 h, (d) after 4 h, (e) after 3 days, (f) after 6 days.

Utilizing the benefits of a catalytic system with only a limited variety of dehydrogenation products, kinetic studies were performed by varying the temperature. These studies were performed in a timeframe between 30 and 240 minutes in order to exclude any influence of a possible induction time and to limit the influence of catalyst decomposition. First, the influence of temperature on the reaction rate was evaluated by performing the

reaction at 50, 60, 70 and 80 °C; the disappearance of DMAB and concomitant appearance of $(NMe_2BH_2)_2$ was followed by ^{11}B NMR spectroscopy over the course of 240 minutes. The plot of ln[DMAB] versus elapsed time (Figure **6**) demonstrated that the reaction is first order in DMAB; the corresponding Arrhenius plot (Figure **7**) allowed us to compute a $\Delta G^{\ddagger}$ of 25.2 kcal/mol at 25 °C via the Eyring-Polanyi equation. This confirms that our DFT model for the reaction of DMAB dehydrogenation is accurate (computed values for dihydrogen abstraction and elimination are 25.1 and 27.3 kcal/mol (ΔG) respectively) and can thus be used for further catalyst design.

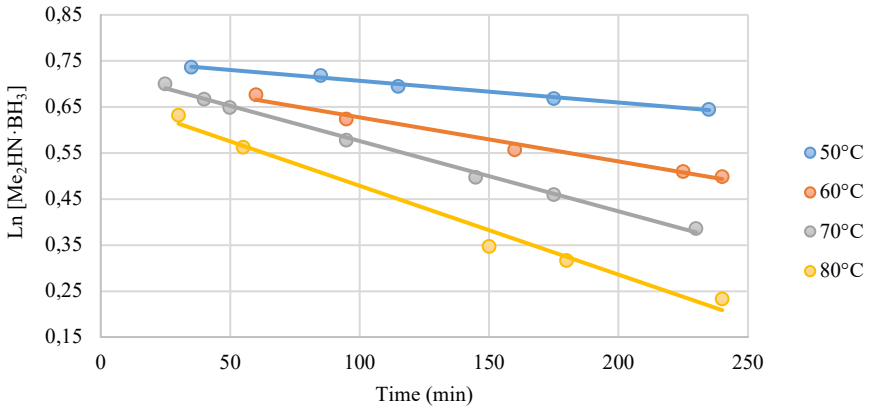

Figure 6. Plot of Ln[DMAB] versus elapsed time for catalytic dehydrogenation reactions of dimethylamine-borane by 4% FLP **6** at different temperatures. Linear curves as $Ln[DMAB]_t = k \cdot t + Ln[DMAB]_0$: 50 °C: $Ln[DMAB] = 4.72 \cdot 10^{-4} t + Ln[2.13]$; 60 °C: $Ln[DMAB] = 9.57 \cdot 10^{-4} t + Ln[2.06]$; 70 °C: $Ln[DMAB] = 15.3 \cdot 10^{-4} t + Ln[2.07]$; 80 °C: $Ln[DMAB] = 19.3 \cdot 10^{-4} t + Ln[1.96]$.

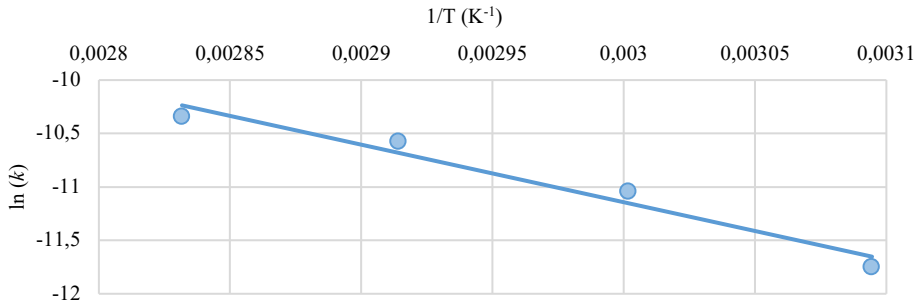

Figure 7. Arrhenius plot of DMAB dehydrogenation by **6** at four temperatures with Ln(k) versus the inverse temperature: $Ln(k) = 5387.07 \cdot (1/T) + 5.01$

The highest turnover number (TON) was obtained with 4 mol% catalyst loading at 70 °C, reaching 23 turnovers after 6 days. The turnover frequency (TOF) after approximately 10% conversion of the dimethylamine-borane substrate at 50 °C was found to be 0.62 h^{-1} which is not high, but is comparable to several transition metal complexes reported by Travieso-Puente and co-workers (Table **1**).[21] As expected, higher TOFs were obtained at higher temperatures and after approximately 10% conversion at 60, 70 and 80 °C TOFs of 1.89, 2.65 and 4.36 h^{-1} were obtained, respectively. At these elevated temperatures also faster catalyst decomposition was observed resulting in lowered turnover frequencies as the conversion increases.

Table 1. Conversion of $Me_2NH{\cdot}BH_3$ in time by **6** and determined TOFs at different temperatures.

Reaction temperature (°C)	t (min)	Conversion (%)	TOF (h^{-1})
50	235	9.3	0.62
60	95	11.4	1.89
70	50	8.4	2.65
80	30	8.3	4.36
80	150	31.1	3.27
80	240	38.5	2.53

Since a minor modification of our original FLP tBu$_2$PCH$_2$BPh$_2$ (**1**) affords tBu$_2$PCH$_2$BMes$_2$ (**6**) that changed the reactivity towards dimethylamine-borane from stoichiometric to catalytic dehydrogenation, we envisioned that additional changes of the P- and B-substituents might further influence the activity of the FLP catalyst. Therefore, we applied a rational catalyst design strategy,[22,23] in which we structurally varied the R and R' substituents *in silico* of the R$_2$PCH$_2$BR'$_2$ core and subsequently studied the influence of these changes on the energy barriers for dihydrogen abstraction (**TS1**) and dihydrogen elimination (**TS2**), as well as on the stabilization of the intermediate H_2-adduct (Figure **8**). Important to note is that the ideal catalyst has a low barrier for dihydrogen abstraction, but should not stabilize the H_2-adduct intermediate too much, since this, most likely, would result in an increased barrier for dihydrogen elimination. Moreover, also the characteristic challenges of

FLP chemistry should be taken into account, as Lewis adduct formation should ideally be avoided as this provides an additional resting state of the catalyst.

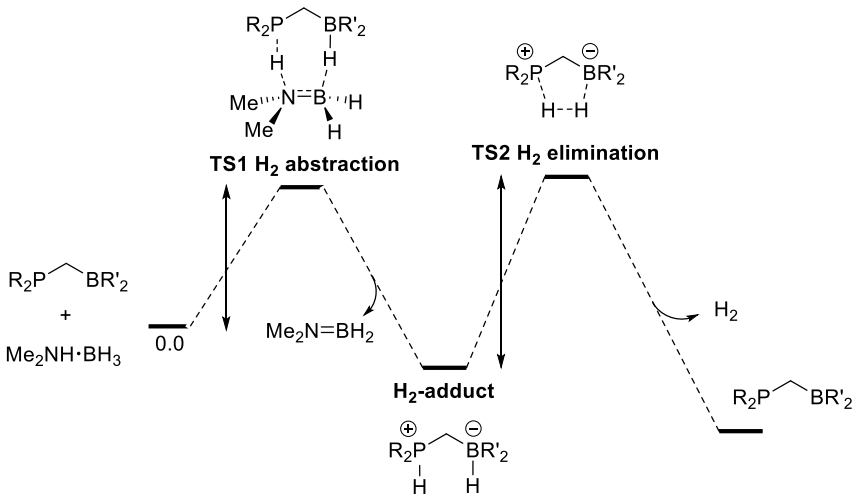

Figure 8. Schematic overview of the two crucial barriers and intermediate during the rational catalyst design for FLP catalyzed amine-borane dehydrogenation.

First, in order to study the effect of the Lewis base moiety of the FLP, the Lewis acidic boron site was kept constant by using the diphenylborane fragment, similar to **1**. The barriers and intermediate were calculated at the ωB97X–D/6-31G* level of theory for a selection of P-substituents (R groups, Figure **9**), varying in size and electronic withdrawing/donation properties. This data revealed that a stronger Lewis base lowers the barrier for dihydrogen abstraction from the amine-borane, but also stabilizes the intermediate H_2 adduct resulting in an increased barrier for H_2 elimination. Interestingly, the size of the substituents did not seem to have a significant effect on the reaction barriers. Encouraged by this initial finding, a second set of computations was performed to study the effect of the Lewis acid by varying the B-substituents for tBu$_2$PCH$_2$BR'$_2$ (R' groups, Figure **9**). These computations reveal that strong Lewis acids significantly lower the barrier for H_2 abstraction, but also highly stabilize the phosphonium-borate intermediate, which makes the release of dihydrogen a high energy

process. These findings indicate that the desired active FLP catalyst features a delicate balance between Lewis acidity and basicity of the borane and phosphine, respectively.

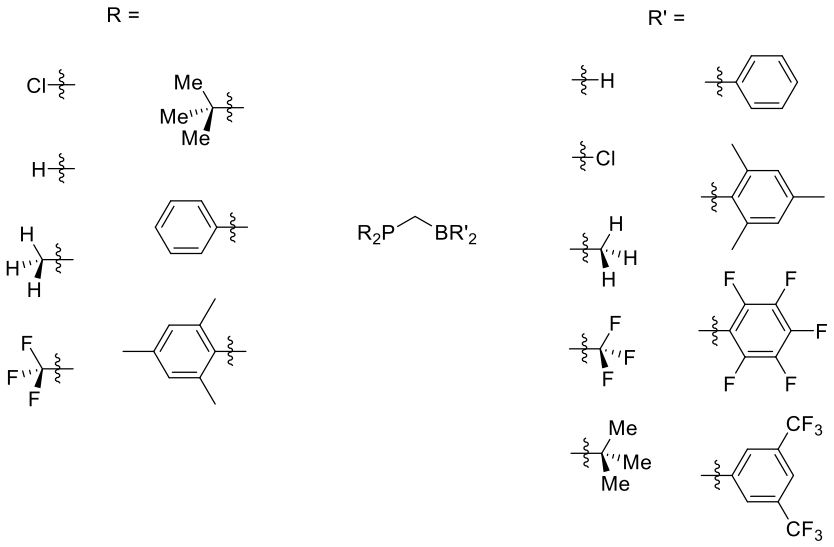

Figure 9. Investigated substituents for the $R_2PCH_2BR'_2$ backbone.

From the initial screening of P-substituents it was found that mesityl substituents are most promising for DMAB dehydrogenation. Although *tert*-butyl substituents would allow faster dihydrogen abstraction as they are stronger donating substituents ($\Delta G^{\ddagger}_{abstraction}$ = 1.7 kcal/mol lower than Mes), they also stabilize formation of the H_2-adduct intermediate. In contrast, the mesityl substituents destabilize this phosphonium-borate intermediate and thereby significantly lower the barrier for dihydrogen elimination resulting in a lower overall barrier ($\Delta G^{\ddagger}_{overall}$ = 3.29 kcal/mol lower than *t*Bu), which highlights the substantial impact of a change of substituents on this FLP system.

Following an iterative process, the new promising FLP backbone $Mes_2PCH_2BR'_2$ bearing mesityl substituents on the phosphorus atom, was subjected to a computational screening of boron substituents (R' groups, Figure **9**) in order to generate a third set of potential FLP catalysts (25 different catalysts in total) for dimethylamine-borane dehydrogenation. These results are depicted in Figure **10**, where each dot represents a unique

FLP catalyst for which the TS (**TS1**) for dihydrogen abstraction is plotted against the TS for dihydrogen elimination (**TS2**), thereby generating a schematic overview of the properties of each individual FLP.

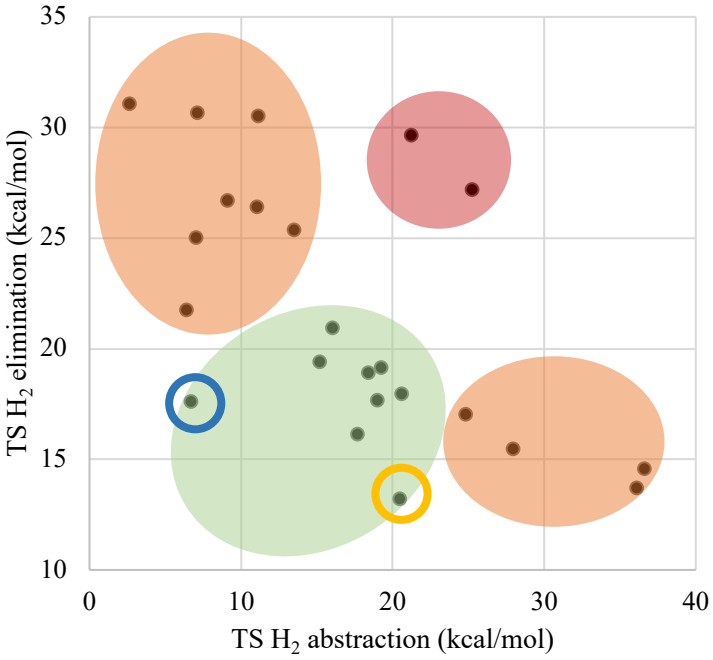

Figure 10. Schematic overview of the barriers in Gibbs free energy for DMAB dehydrogenation for all investigated FLPs.

From figure **10**, some observations can be made: 1) highlighted in red, FLPs possessing a bulky *tert*-butyl P-substituent in combination with a bulky Lewis acid (*t*Bu, Mes) possess a high energy barrier for both dihydrogen abstraction and elimination. 2) FLPs with a high barrier for dihydrogen abstraction (orange highlight, bottom right) contain an electron poor phosphine moiety, such as Cl_2P-R, which results in poor proton accepting properties of the Lewis base and therefore a high barrier for H_2 abstraction. 3) FLPs containing a strong Lewis acid (orange highlight, top left) were found to have a high barrier for H_2 elimination, which

can be explained by the substantial increased stabilization of the phosphonium-borate intermediate.

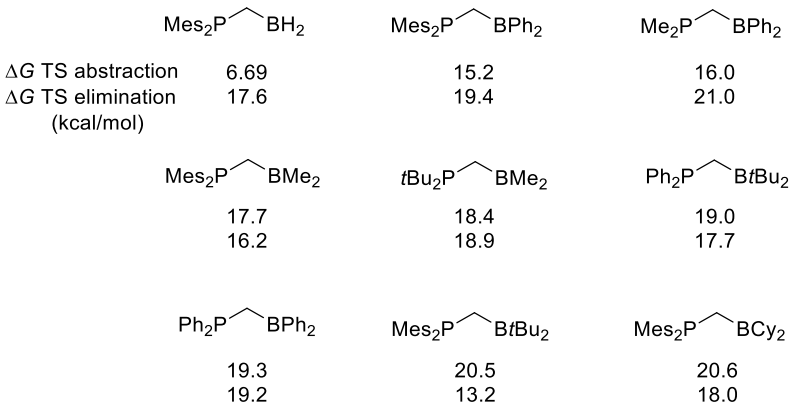

Figure 11. Potential hits for catalytic dehydrogenation of DMAB and their corresponding energy barriers (ΔG) for dihydrogen abstraction and elimination.

Highlighted in green in figure **10** are the most interesting hits for catalytic dehydrogenation of dimethylamine-borane, since these FLPs contain a low barrier for both dihydrogen abstraction and elimination (Figure **11**). It is important to note, though, that not only these two transition states should be considered as rate limiting steps during catalysis, the ideal catalyst should also prevent FLP dimerization, formation of 5-membered heterocycles, such as **3** or **8**, and BH_3 exchange from the amine-borane. For example, the blue encircled FLP (Figure **10**) represents $Mes_2PCH_2BH_2$ which is an interesting candidate, also as it is an analogue of the *ortho*-phenylene bridged amine-borane FLP $R_2NC_6H_4BH_2$ that has been widely applied by Fontaine et al. for a variety of bond activations.[24,25] However, due to the lack of steric hindrance at the borane center, $Mes_2PCH_2BH_2$ favors the formation of the 5-membered heterocycle, comparable to **3** and **8**, which would significantly decrease or completely remove the catalytic activity. Very interestingly, $Mes_2PCH_2BtBu_2$ (**8**) (Figure **10**, circled in orange) bearing a moderately donating Lewis base and a very weak Lewis acid, was found to be another potential hit from our computational survey. This finding can be rationalized as the mesityl substituents on phosphorus makes the phosphine just basic enough

to allow rapid dihydrogen abstraction from dimethylamine-borane ($\Delta G^{\ddagger}_{abstraction}$ = 20.5 kcal/mol, $\Delta E^{\ddagger}_{abstraction}$ = 8.24 kcal/mol). Moreover, the *tert*-butyl substituent on boron highly destabilize the phosphonium-borate intermediate (ΔG = 5.93 kcal/mol, ΔE = 9.12 kcal/mol) making the elimination of dihydrogen a low energy barrier process ($\Delta G^{\ddagger}_{elimination}$ = 13.2 kcal/mol, $\Delta E^{\ddagger}_{elimination}$ = 16.7 kcal/mol). Potential side reactions such as FLP dimerization, the reaction with generated amino-borane $Me_2N{=}BH_2$, and BH_3 exchange were all found to be endergonic.

With $Mes_2PCH_2BtBu_2$ (**8**) as synthetic target, a synthetic challenge emerged as the needed building block Mes_2PCH_2Li is synthetically unavailable. Therefore, a new synthesis was envisioned in which the C_1-linker of the FLP is first installed at the boron site giving **9**, which could be used to connect the mesityl-substituted phosphine moiety (Scheme **5**). Additionally, alkoxy substituents on the borane starting material could allow late-stage functionalization of the Lewis acid, which could be beneficial for further derivatization of the FLP.

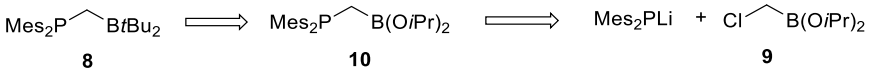

Scheme 5. Retrosynthesis of synthetic target FLP **8**.

9 was synthesized in moderate yield (63%) using a modified procedure reported by Brown an co-workers,[26] which allows replacement of one isopropoxy group of triisopropylborate for a $–CH_2Cl$ moiety using iodochloromethane and methyllithium (Scheme **6**). Installation of the dimesitylphosphine moiety was achieved by a salt metathesis reaction between **9** and Mes_2PLi, which afforded the FLP precursor **10** as a colorless oil in 77% yield. In order to synthesize the final product **8**, we attempted to displace the two isopropoxy groups in **10** by using *t*BuMgBr as alkylating agent, but no conversion to the desired product was observed. In contrast, *tert*-butyllithium was found to be suited for this reaction and could easily convert **10** to the final product **8**.

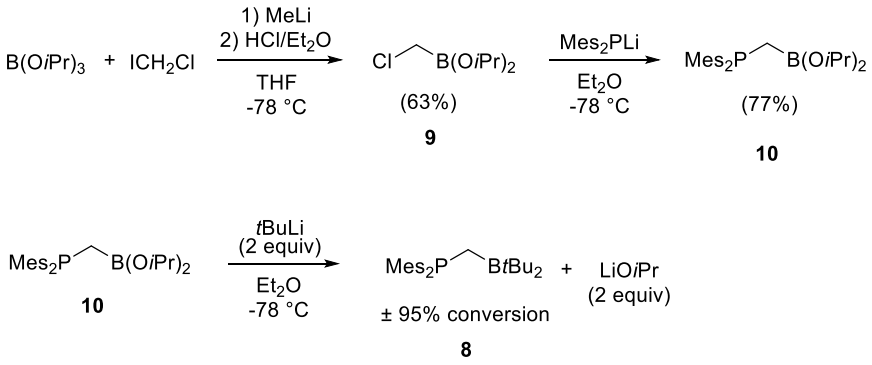

Scheme 6. Synthesis of target FLP **8**.

The drawback of this reaction is, however, the concomitant formation of 2 equivalents of lithium isopropoxide, which prevented isolation of pure product. Attempts to remove lithium isopropoxide by filtration were unsuccessful, as the salt is soluble in nonpolar solvents such as *n*-pentane. FLP **8** did not allow quenching of the lithium isopropoxide with HCl/Et_2O or TMSCl, since **8** decomposes under these conditions. Additionally, attempts to precipitate lithium isopropoxide by the addition of trialkylborates, 12-crown-4, salts (for metathesis), or metal complexes were all ineffective or led to product decomposition.

In order to avoid the formation of alkoxy salts, we envisioned that the borane moiety should be functionalized prior to the introduction of the phosphine, while keeping the C_1-linker installed at the boron site. **11** (Scheme **7**) is therefore is suitable precursor, which might be deprotonated to form the lithiated species **12**, as the analogous nucleophile $LiCH_2BMes_2$ is well documented.[27] Finally, **12** could be reacted with the needed chlorophosphine Mes_2PCl to afford the target FLP **8**. This new strategy for the synthesis of **8** is currently under investigation in our laboratory.

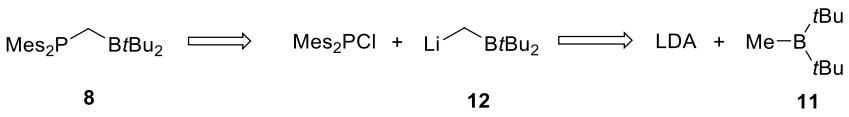

Scheme 7. A second approach towards the synthesis of target FLP **8**.

2.3 Conclusion

In summary, tBu$_2$PCH$_2$BPh$_2$ (**1**) conveniently dehydrogenates ammonia-borane and dimethylamine-borane to form the FLP-H$_2$ adduct **2** and a new 5-membered heterocycle (**3** or **5**, respectively). DFT calculations revealed that the underlying mechanism operates via formation of a three-center-two-electron adduct, which is followed by a concerted double hydrogen abstraction step involving a 7-membered transition state. The more bulky FLP tBu$_2$PCH$_2$BMes$_2$ (**6**) was designed and subsequently synthesized in excellent yields. **6** shows catalytic activity towards ammonia-borane, and kinetic studies on the dehydrogenation of Me$_2$NH·BH$_3$ showed first order kinetics towards the substrate and turn over numbers and frequencies up to 23 and 4.36 h^{-1}, respectively. Rational catalyst design was applied to create a more active catalyst and Mes$_2$PCH$_2$BtBu$_2$ (**8**) was found as highly potential catalyst. The synthesis of this new catalyst is currently under development in our laboratories.

2.4 Experimental Details

All manipulations were carried out under an atmosphere of dry nitrogen, using standard Schlenk and drybox techniques. Solvents were purified, dried and degassed according to standard procedures and stored under 3Å molecular sieves or a sublimed sodium mirror. ^{1}H and ^{13}C{^{1}H} NMR spectra were recorded on a Bruker Avance 400 or Brucker Avance 500 and internally referenced to the residual solvent resonances (CDCl$_3$: ^{1}H δ 7.26, ^{13}C{^{1}H} δ 77.2; THF-d_8: ^{1}H δ 3.58, 1.72, ^{13}C{^{1}H} δ 67.2, 25.3; C$_6$D$_6$: ^{1}H δ 7.16, ^{13}C{^{1}H} 128.1; Tol-d_8: ^{1}H δ 7.09, 7.01, 6.97, 2.08, ^{13}C{^{1}H} δ 137.48, 128.87, 127.96, 125.13, 20.43). ^{31}P{^{1}H}, ^{31}P, ^{11}B{^{1}H} and ^{11}B NMR spectra were recorded on a Bruker Avance 400 and externally referenced (85% H$_3$PO$_4$, BF$_3$·OEt$_2$, respectively). High resolution mass spectra were recorded on a Bruker MicroTOF with ESI nebulizer (ESI). Melting points were measured in sealed capillaries and are uncorrected. tBu$_2$PCH$_2$Li,[28] and tBu$_2$PCH$_2$BPh$_2$ (**1**)[14a] were synthesized following literature procedures. 2-MeTHF was purchased from Sigma Aldrich and subsequently degassed and dried with 3Å molecular sieves. NH$_3$·BH$_3$, NHMe$_2$·BH$_3$, PBr$_3$, MesMgBr (1M in THF), LiAlH$_4$, n-BuLi (1.6M in hexane), t-BuLi (1.7M in pentane), MeLi (1.6M in Et$_2$O), BCl$_3$ (1 M in heptane) and B(OMe)$_3$ were purchased from Sigma

Aldrich, CH_2ICl was purchased from VWR International B.V., and all were used without any further purification.

Preparation of *t*$Bu_2PCH_2BPh_2$-H_2 adduct 2:[14a]

A THF stock solution of ammonia-borane (28.84 mL, 0.1 M, 2.88 mmol, 1.0 equiv) was added to a solution of *t*$Bu_2PCH_2BPh_2$ (**1**, 1.87 gr, 5.77 mmol, 2.0 equiv) in THF (15 mL) at 0 °C. After addition, the reaction mixture was warmed to room temperature and all volatiles were removed *in vacuo*. The obtained colorless solid was thoroughly washed with *n*-pentane (3 x 20 mL) and the solids were subsequently dried *in vacuo* to afford **2** as a colorless solid (0.536 g, 57%). Colorless X-ray quality crystals were obtained from a solution of **2** in *n*-pentane which was stored at 4 °C.

^{1}H NMR (400.13 MHz, THF-*d*$_8$, 293 K): δ 7.32 (d, $^3J_{H,H}$ = 7.1 Hz, 4H; *o*-Ph*H*), 6.97 (t, $^3J_{H,H}$ = 7.4 Hz, 4H; *m*-Ph*H*), 6.82 (t, $^3J_{H,H}$ = 7.3 Hz, 2H; *p*-Ph*H*), 4.96 (dt, $^1J_{H,P}$ = 453.2 Hz, $^3J_{H,H}$ = 4.8 Hz, 1H; P*H*), 3.12–2.29 (br. m, 1H; B*H*), 1.26 (d, $^3J_{H,P}$ = 14.8 Hz, 18H; C(CH_3)$_3$), 1.19–1.10 (br. m, 2H; PCH_2B).

^{31}P{^{1}H} NMR (162.0 MHz, THF-*d*$_8$, 293 K): δ –10.1 (s).

^{11}B{^{1}H} NMR (128.4 MHz, THF-*d*$_8$, 293 K): δ 59.0 (s).

Preparation of *t*$Bu_2PCH_2BPh_2$-NH_2BH_2 adduct 3:

A THF stock solution of ammonia-borane (28.84 mL, 0.1 M, 2.88 mmol, 1.0 equiv) was added to a solution of *t*$Bu_2PCH_2BPh_2$ (**1**, 1.87 gr, 5.77 mmol, 2.0 equiv) in THF (15 mL) at 0 °C. After addition, the reaction mixture was warmed to room temperature and all volatiles were removed *in vacuo*. The obtained white solid was thoroughly extracted in *n*-pentane (3 x 20 mL). The combined extracts were filtered over a pad of alumina, which was subsequently flushed with 250 mL eluent (cyclohexane/ethyl acetate 20:1, resp.). The collected filtrate was dried *in vacuo* to afford **3** as a colorless solid (0.754 g, 74%). X-ray quality crystals were obtained from a solution of **3** (289 mg) in a pentane/DCM mixture (7.5 mL : 0.54 mL) which was stored at 4 °C.

Melting point (nitrogen, sealed capillary): 128 °C.

^{1}H NMR (400.13 MHz, THF-*d*$_8$, 293 K): δ 7.29 (d, $^{3}J_{H,H}$ = 7.1 Hz, 4H; *o*-Ph*H*), 7.03, (t, $^{3}J_{H,H}$ = 7.4 Hz, 4H; *m*-Ph*H*), 6.89 (t, $^{3}J_{H,H}$ = 7.2 Hz, 2H, *p*-Ph*H*), 3.37 (br. s, 2H; NH_2), 2.80–1.75 (br. m, 2H; BH_2), 1.19–1.13 (m, 20H; PCH_2B, C(CH_3)$_3$).

^{13}C{^{1}H} NMR (100.62 MHz, THF-*d*$_8$, 293 K): δ 157.0 (br. s; *ipso*-Ph*C*), 132.1 (s; *o*-Ph*C*), 127.2 (s; *m*-Ph*C*), 124.4 (s; *p*-Ph*C*), 31.8 (d; $^{1}J_{C,P}$ = 25.8 Hz; *C*(CH$_3$)$_3$), 28.1 (d; $^{2}J_{C,P}$ = 1.2 Hz; C(*C*H$_3$)$_3$), 9.0 (s; PCH_2B).

^{31}P{^{1}H} NMR (162.0 MHz, THF-*d*$_8$, 293 K): δ 56.7 (br. m).

^{11}B{^{1}H} NMR (128.4 MHz, THF-*d*$_8$, 293 K): δ –1.95 (s; *B*Ph$_2$), –20.7 (d, $^{1}J_{B,P}$ = 85.5 Hz; P*B*H$_2$N).

HR–MS (ESI): 352.2554 [**3**–H]$^{+}$, calcd for: $C_{21}H_{33}B_2NP^{+}$ 352.25312.

Preparation of Mes$_2$BOMe:[29]

A solution of MesMgBr (1 M in THF, 27 mL, 27 mmol, 2.1 equiv) was added dropwise to a solution of B(OMe)$_3$ (1.45 mL, 1.35 g, 13 mmol, 1.0 equiv) in THF (15 mL), which resulted in a grey suspension that turned into a brown solution after heating to 55 °C for 5h and subsequent stirring at room temperature overnight. The volatiles were removed *in vacuo* and the mixture was extracted into *n*-pentane (40 + 18 mL). The combined extracts were dried *in vacuo* to yield a colorless solid (2.98 g, 82%). Crystallization of this compound was possible from a solution in hot methanol (10 mL/g product) to afford colorless crystals upon cooling.

^{1}H NMR (500.23 MHz, CDCl$_3$, 293 K): δ 6.79 (s, 4H; Mes*H*), 3.75 (s, 3H; OCH_3), 2.27 (s, 6H; *p*-MesCH_3), 2.22 (s, 12H; *o*-MesCH_3).

^{13}C{^{1}H} NMR (125.80 MHz, CDCl$_3$, 293 K): δ 128.3 (br. s; *m*-Mes*C*), 54.3 (s; O*C*H$_3$), 22.4 (s; *o*-Mes*C*H$_3$), 21.3 (s; *p*-Mes*C*H$_3$), the signals for *ipso*-Mes*C*, *o*-Mes*C* and *p*-Mes*C* are unresolved.

^{11}B{^{1}H} NMR (128.38 MHz, CDCl$_3$, 293 K): δ 45.0 (br. s).

Preparation of Mes$_2$BCl:[30]

A solution of BCl_3 (1 M in heptane, 19 mL, 19 mmol, 1.3 equiv) was added dropwise to a solution of Mes$_2$BOMe (4.13 g, 14.8 mmol, 1.0 equiv) in heptane (20 mL) at room temperature, after which the mixture was heated overnight at 60 °C. The reaction mixture was cooled to room temperature and the volatiles were removed *in vacuo* to offer pinkish

solids that were extracted into *n*-pentane (12 + 20 mL). The combined extracts were dried *in vacuo*, which afforded a colorless solid (3.86 g, 92%). X-ray quality crystals were obtained by recrystallization from hot pentane (2.6 mL/g crude Mes_2BCl) and subsequent washing with pentane (0.5 mL/g crude) at –80 °C to afford colorless crystals.

Melting point (nitrogen, sealed capillary): 80–84°C (trajectory).

^{1}H NMR (500.23 MHz, $CDCl_3$, 293 K): δ 6.83 (s, 4H; Mes-*H*), 2.30 (s, 12H; *o*-MesCH_3), 2.28 (s, 6H; *p*-MesCH_3).

^{13}C{^{1}H} NMR (125.80 MHz, $CDCl_3$, 293 K): δ 140.9 (s; *o*-Mes*C*), 140.5 (s; *p*-Mes*C*), 129.0 (s; *m*-Mes*C*), 23.4 (s; *o*-Mes*C*H_3), 21.4 (s; *p*-Mes*C*H_3), the signal for *ipso*-Mes*C* is unresolved.

^{11}B{^{1}H} NMR (128.38 MHz, $CDCl_3$, 293 K): δ 69.9 (br. s).

Preparation of *t*$Bu_2PCH_2BMes_2$ (6):

A solution of Mes_2BCl (3.47 g, 12.2 mmol, 1.0 equiv) in Et_2O (15 mL) was added dropwise to a suspension of *t*Bu_2PCH_2Li (2.72 g, 16.4 mmol, 1.3 equiv) in Et_2O (15 mL) at –80 °C and after addition the reaction mixture was warmed to room temperature. After 2.5 days of stirring at room temperature, the suspension was concentrated *in vacuo* which afforded an orange foam. The foam was extracted into *n*-pentane (25 mL) and filtrated over a Schlenk filter packed with celite. Subsequently, the celite layer was extracted into pentane (3 x 10 mL) and the combined extracts were concentrated *in vacuo*, which afforded an orange solid (4.94 g, 99%). X-ray quality crystals were obtained from a solution of 0.45 g of **6** in 1 mL of hot heptane (80–85 °C) and subsequent slow cooling to –20 °C.

Melting point (nitrogen, sealed capillary): 79–87 °C (trajectory).

^{1}H NMR (400.13 MHz, C_6D_6, 293 K): δ 6.77 (s, 4H; Mes*H*), 2.43 (s, 12H; *o*-MesCH_3), 2.15 (s, 6H; *p*-MesCH_3), 2.09 (d, $^2J_{H,P}$ = 4.7 Hz, 2H; PCH_2B), 1.08 (d, $^2J_{H,P}$ = 10.5 Hz, 18H; C(CH_3)$_3$).

^{13}C{^{1}H} NMR (100.62 MHz, C_6D_6, 293 K): δ 143.4 (only observed in the HMBC spectrum, $^3J_{C,H}$ coupling with Mes*H*, *o*-MesCH_3, and PCH_2B; *ipso*-Mes*C*), 139.1 (s; *o*-Mes*C*), 138.3 (s; *p*-Mes*C*), 129.2 (s; *m*-Mes*C*), 31.5 (d, $^1J_{C,P}$ = 25.1 Hz; *C*(CH_3)$_3$), 30.0 (d, $^1J_{C,P}$ = 14.1 Hz; C(*C*H_3)$_3$), 28.1 (only observed in the HSQC spectrum, $^1J_{C,H}$ coupling with PCH_2B; P*C*H_2B), 24.1 (2 x s; *o*-Mes*C*H_3), 21.2 (s; *p*-Mes*C*H_3).

$^{31}P\{^{1}H\}$ NMR (161.97 MHz, toluene-d_8, 293 K): δ 26.9 (s).

$^{11}B\{^{1}H\}$ NMR (128.38 MHz, toluene-d_8, 293 K): δ 82.0 (br. s).

HR–MS (ESI): 409.3200 [**6**+H]$^+$, calcd for $C_{27}H_{43}BP^+$ 409.3190.

Preparation of Mes_2PBr:

A solution of MesMgBr (1M in THF, 42.6 mL, 42.6 mmol, 2 equiv) was dropwise added to a solution of PBr_3 (5.76 g, 2 mL, 21.3 mmol, 1 equiv) in Et_2O (20 mL) at –78 °C. After addition the reaction mixture was warmed to room temperature and stirred overnight which afforded a thick suspension. The solvent was removed *in vacuo* and the solids were extracted into toluene (3 x 40 mL). The combined extracts were dried *in vacuo* which afforded a thick oil which solidified into a yellow solid (8.18 g). The yellow solid was extracted into Et_2O and the combined extracts were subsequently dried *in vacuo* to afford a yellow oil which solidified into a yellow solid (6.93 g, 93%).

^{1}H NMR (400.13 MHz, THF-d_8, 297 K): δ 6.83 (d, $^{4}J_{H,P}$ = 3.4 Hz, 4H; Mes*H*), 2.33 (d, $^{4}J_{H,P}$ = 2.4 Hz, 12H; *o*-MesC*H*$_3$), 2.24 (s, 6H; *p*-MesC*H*$_3$).

$^{31}P\{^{1}H\}$ NMR (161.97 MHz, THF-d_8, 297 K): δ 75.1 (s).

Preparation of Mes_2PH:

A solution of Mes_2PBr (6.89 g, 19.7 mmol, 1 equiv) in Et_2O (40 mL) was added dropwise to a suspension of $LiALH_4$ (0.374 g, 9.86 mmol, 0.5 equiv) in Et_2O (40 mL) at room temperature. After addition, the reaction mixture was stirred for 1 hour at room temperature after which H_2O (40 mL, 2.2 mol) and HCl (2M in Et_2O, 30 mL, 60 mmol) were added. The organic phase was separated and the water phase was extracted with Et_2O (3 x 20 mL) and the combined extracts were dried over $MgSO_4$, filtered and the solvent was removed *in vacuo* which afforded a colorless solid (4.66 g, 88%). If necessary, the product can be crystallized by cooling a solution of Mes_2PH in *n*-pentane to –20 °C.

^{1}H NMR (400.13 MHz, C_6D_6, 298 K): δ 6.69 (s, 4H; Mes*H*), 5.32 (d, $^{1}J_{H,P}$ = 229.5 Hz, 1H; P*H*), 2.27 (s, 12H; *o*-MesC*H*$_3$), 2.08 (s, 6H; *p*-MesC*H*$_3$).

^{31}P NMR (161.97 MHz, C_6D_6, 298 K): δ –93.1 (d, $^{1}J_{H,P}$ = 229.5 Hz).

$^{31}P\{^{1}H\}$ NMR (161.97 MHz, C_6D_6, 298 K): δ –93.1 (s).

Preparation of Mes_2PLi:

A solution of *n*-BuLi (1.6 M in hexane, 4.0 mL, 6.42 mmol, 1.15 equiv) was added to a solution of Mes_2PH (1.509 g, 5.58 mmol, 1 equiv) in pentane (25 mL) at 0 °C. After addition, the mixture was warmed to room temperature and stirred for 3 days which afforded a yellow suspension. The suspension was filtered and the solids were washed with *n*-pentane (3 x 20 mL). The solids were subsequently dried *in vacuo* to afford a red solid (1.38 g, 89%).

^{1}H NMR (400.13 MHz, THF-d_8, 298 K): δ 6.50 (s, 4H; Mes*H*), 2.10 (s, 12H; *o*-MesCH_3), 2.24 (s, 6H; *p*-MesCH_3).

^{31}P{^{1}H} NMR (161.97 MHz, THF-d_8, 298 K): δ –63.5 (s).

Preparation of $ClCH_2B(OiPr)_2$ (9):

A solution of MeLi (1.65M in Et_2O, 29.1 mL, 48 mmol, 1 equiv) was slowly added to a solution of CH_2ICl (8.56 g, 3.61 mL, 48 mmol, 1 equiv) and $B(OiPr)_3$ (9.03 g, 11.1 mL, 48 mmol, 1 equiv) in THF (30 mL) at –78 °C. After addition, the mixture was stirred at –78 °C for 45 minutes, and subsequently warmed to room temperature which afforded a suspension. The suspension was cooled to 0 °C and a solution of HCl (2M in Et_2O, 25 mL, 50 mmol, 1.04 equiv) was added. The reaction mixture was warmed to room temperature, filtered and carefully concentrated under reduced pressure. Fractional distillation through a short Vigreux column yielded a colorless liquid (5.43 g, 63%).

^{1}H NMR (400.13 MHz, $CDCl_3$, 297 K): δ 4.46 (hept, $^3J_{H,H}$ = 6.1 Hz, 2H; OC*H*$(CH_3)_2$), 2.89 (s, 2H; BCH_2Cl), 1.20 (d, $^3J_{H,H}$ = 6.1 Hz, 12H; OCH$(CH_3)_2$).

^{11}B{H} NMR (128.38 MHz, $CDCl_3$, 297 K): δ 26.7 (s).

Preparation of $Mes_2PCH_2B(OiPr)_2$ (10):

A solution of Mes_2PLi (0.429 g, 1.55 mmol, 1 equiv) in Et_2O (15 mL) was slowly added to a solution of $ClCH_2B(OiPr)_2$ at –78 °C. After addition, the clear yellow reaction mixture was kept for 15 minutes at –78 °C and subsequently warmed to room temperature which afforded colorless suspension. The solvent was removed *in vacuo* and the product was extracted into *n*-pentane (3 x 5 mL) and the combined extracts were dried *in vacuo* which afforded a colorless oil (0.49 g, 77%).

^{1}H NMR (400.13 MHz, C_6D_6, 297 K): δ 6.69 (d, $^{4}J_{H,P}$ = 2.3 Hz, 4H; Mes*H*), 4.43 (hept, $^{2}J_{H,H}$ = 6.1 Hz, 2H; OC*H*(CH_3)$_2$), 2.43 (s, 12H; *o*-MesCH_3), 2.17 (s, 2H; PCH_2B), 2.09 (s, 6H; *p*-MesCH_3), 1.04 (d, $^{3}J_{H,H}$ = 6.1 Hz, 12H; OCH(CH_3)$_2$).

^{13}C{^{1}H} NMR (100.62 MHz, C_6D_6, 298 K): δ 142.0 (d, $^{2}J_{C,P}$ = 14.2 Hz; *o*-Mes*C*), 137.2 (s; *p*-Mes*C*), 135.3 (d, $^{1}J_{C,P}$ = 25.0 Hz; *ipso*-Mes*C*), 130.4 (d, $^{3}J_{C,P}$ = 2.7 Hz; *m*-Mes*C*), 65.8 (s, O*C*H(CH_3)$_2$), 24.6 (s; OCH(*C*H_3)$_2$), 23.3 (d, $^{3}J_{C,P}$ = 14.3 Hz; *o*-Mes*C*H_3), 20.9 (s; *p*-Mes*C*H_3), 13.6 (only observed in the HSQC spectrum, $^{1}J_{C,H}$ coupling with PCH_2B; P*C*H_2B).

^{31}P{^{1}H} NMR (161.97 MHz, C_6D_6, 298 K): δ –27.7 (s).

^{11}B{^{1}H} NMR (128.38 MHz, C_6D_6, 298 K): δ 29.4 (s).

Preparation of crude $Mes_2PCH_2Bt Bu_2$ (8):

A typical procedure for the synthesis of $Mes_2PCH_2Bt Bu_2$ purification:

A solution of *t*-BuLi (1.7M in pentane, 0.54 mL, 0.92 mmol, 2 equiv) was slowly added to a solution of $Mes_2PCH_2B(OiPr)_2$ (0.190 g, 0.46 mmol, 1 equiv) in Et_2O (10 mL) at –78 °C which afforded a yellow solution. The reaction mixture was warmed to room temperature, the solvent was removed and the product was extracted in *n*-pentane (5 mL). The solvent was removed *in vacuo* to yield the crude product.

^{31}P{^{1}H} NMR (161.97 MH, *n*-pentane, 294 K): δ –27.9 (s).

^{11}B{H} NMR (128.38 MHz, *n*-pentane, 294 K): δ –85.5 (br. s).

From this point the product is still contaminated with approximately 2 equivalents of lithium isopropoxide, as this is also soluble in *n*-pentane. Various attempts were made from this stage to quench or trap the lithium isopropoxide, which all led to decomposition of the product.

Stability of $tBu_2PCH_2BPh_2$-H_2 adduct (2) towards heating:

A NMR sample containing a solution of **2** in 2-MeTHF was heated to 50 °C for 3 hours, after which ^{31}P{^{1}H} spectroscopy revealed no formation of $tBu_2PCH_2Ph_2$ and only 2% decomposition to tBu_2PCH_3. Subsequent heating to 80 °C for 2 hours resulted in liberation of dihydrogen and 17% conversion to $tBu_2PCH_2Ph_2$ as well as 18% decomposition to tBu_2PCH_3.

Reaction of *t*Bu$_2$PCH$_2$BMes$_2$ (6) with 0.5 equivalents of NH$_3$BH$_3$:

A screw-cap NMR tube was charged with ammonia-borane (0.0054 g, 0.175 mmol, 1.0 equiv), *t*Bu$_2$PCH$_2$BMes$_2$ (**6**, 0.1428 g, 0.350 mmol, 2.0 equiv) and 2-MeTHF (6 mL). The reaction mixture was kept at room temperature and analyzed after 1 hour with ^{31}P{^{1}H}, ^{11}B{^{1}H} and ^{11}B NMR spectroscopy, showing a mixture of dehydrogenated ammonia-borane products (^{11}B{^{1}H} NMR: δ 30.8 (borazine), –4.94 (BCDB), –11.2 (CTB)), along with the formation of the H$_2$-adduct **7** (^{11}B NMR: δ –15.0 (d, $^1J_{B,H}$ = 81.1 Hz); ^{31}P{^{1}H} NMR: δ 56.5 (s)) and 5-membered heterocycle **8** (^{11}B NMR: δ 1.92 (s), –23.3 (t, $^1J_{B,H}$ = 72.9 Hz); ^{31}P{^{1}H} NMR: δ 58.1 (br. s)). Subsequently, the reaction mixture was heated to 70 °C overnight and a white suspension was obtained (solids are postulated to be polyborazine) and ^{31}P{^{1}H}, ^{11}B and ^{11}B{^{1}H} NMR spectroscopy revealed complete consumption of the H$_2$-adduct **7** and heterocycle **8**, as well as an increase in formation of borazine, polyborazine (^{11}B NMR: δ 24.8 (s)), formation of two unidentified products (^{11}B NMR: δ –23.4 (s) and –29.8 (s)), decomposition to Mes$_2$B=NH$_2$ (^{11}B NMR: δ 43.7 (s)) and tBu$_2$PCH$_3$·BH$_3$ (^{11}B NMR: δ –41.6 (dq, $^1J_{B,H}$ = 96.4 Hz, $^1J_{B,P}$ = 57.9 Hz; ^{31}P{^{1}H} NMR: δ 39.9 (br. q), and lastly also regeneration of FLP **6**.

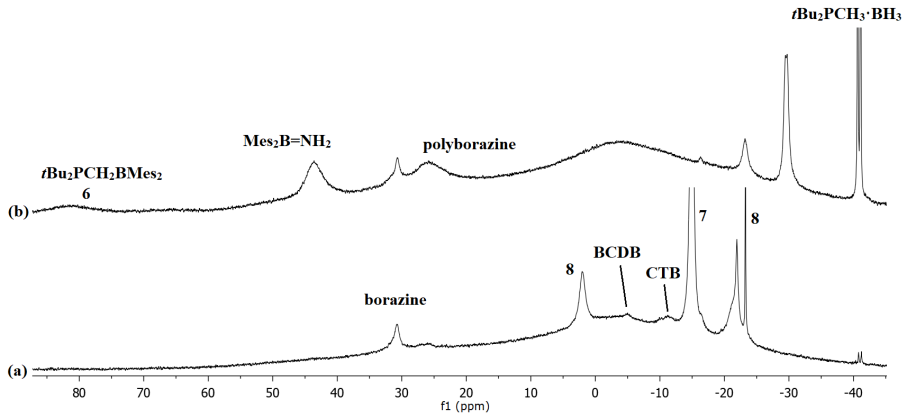

Figure 11. ^{11}B{^{1}H} NMR spectra of (a) ammonia-borane and **6** mixed in a 1:2 ratio after 1h at room temperature in 2-MeTHF, and (b) the reaction mixture after heating to 70 °C overnight.

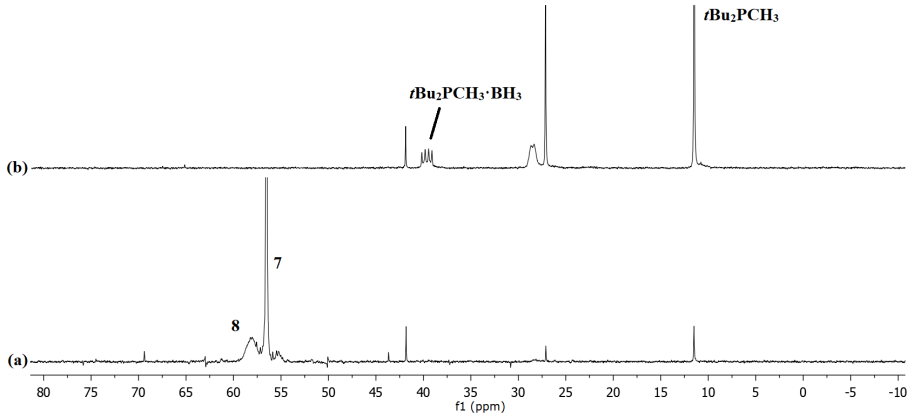

Figure 12. $^{31}P\{^{1}H\}$ NMR spectra of (a) ammonia-borane and **6** mixed in a 1:2 ratio after 1h at room temperature in 2-MeTHF, and (b) the reaction mixture after heating to 70 °C overnight.

Reaction of *t*Bu$_2$PCH$_2$BMes$_2$ (6) with 25 equivalents of NH$_3$BH$_3$:

A screw-cap NMR tube was charged with ammonia-borane (0.031 g, 1.357 mmol, 25.0 equiv), *t*Bu$_2$PCH$_2$BMes$_2$ (**6**, 0.022 g, 0.054 mmol, 1.0 equiv) and 2-MeTHF (6 mL). The reaction mixture was mixed at room temperature and directly analyzed by $^{31}P\{^{1}H\}$, $^{11}B\{^{1}H\}$ and ^{11}B NMR spectroscopy, which revealed formation of the H$_2$-adduct **7** and the 5-membered heterocycle **8**. Subsequently, the NMR tube was heated to 70 °C and analyzed by NMR spectroscopy after 20 and 120 minutes, after which complete consumption of FLP **6** and H$_2$-adduct **7** was observed, along with the formation of dehydrogenation products and dihydrogen gas.

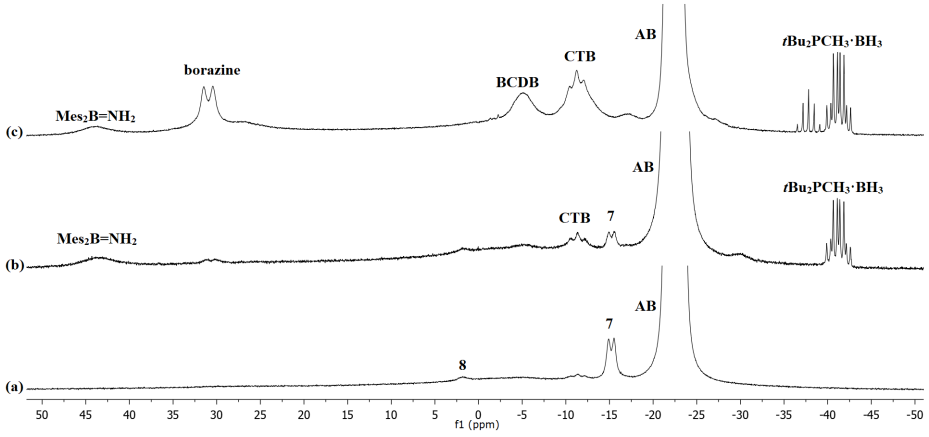

Figure 13. ^{11}B NMR spectra of ammonia-borane mixed with 4% of FLP **6** in 2-MeTHF (a) after mixing at room temperature, (b) 20 minutes at 70 °C, and (c) 120 minutes at 70 °C.

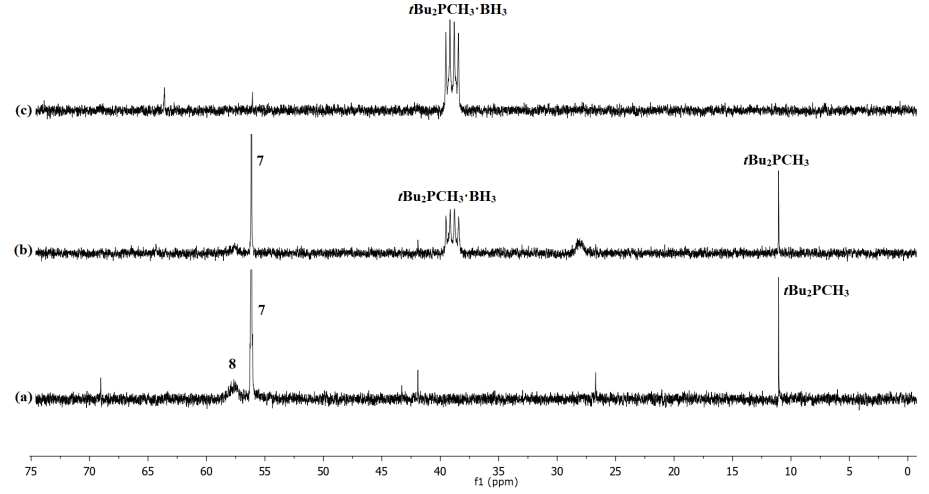

Figure 14. ^{31}P{^{1}H} NMR spectra of ammonia-borane mixed with 4% of FLP **6** in 2-MeTHF (a) after mixing at room temperature, (b) 20 minutes at 70 °C, and (c) 120 minutes at 70 °C.

Kinetic studies on catalytic dehydrogenation of $Me_2NH{\cdot}BH_3$ with FLP 6:

General method:

A screw-cap NMR tube equipped with an sealed capillary containing $B(OMe)_3$ as internal standard was charged with a defined amount of FLP **6**, and 0.5 mL of a stock solution of $Me_2NH{\cdot}BH_3$ (1.05 mmol, 2.1 M in 2-MeTHF). The reaction tube was heated to the desired temperature and the cap was opened under nitrogen atmosphere, to prohibit any H_2 pressure buildup in the system. The progress of the reaction was followed by ^{11}B (128.38 MHz, 293 K) and $^{31}P\{^1H\}$ (161.97 MHz, 293 K) NMR spectroscopy.

4% FLP 6, 50 °C. As described in the general method; 16.5 mg of FLP (0.04 mmol) was mixed with 61.9 mg (1.05 mmol) of $Me_2HN{\cdot}BH_3$ at 50 °C. NMR spectra were recorded after addition, 10, 35, 85, 115, 170, 240 minutes at 50 °C.

4% FLP 6, 60 °C. As described in the general method; 16.4 mg of FLP (0.04 mmol) was mixed with 62.1 mg (1.05 mmol) of $Me_2HN{\cdot}BH_3$ at 60 °C. NMR spectra were recorded after addition, 20, 60, 95, 160, 225, 240, 1710, 1765, 1815, 1860 minutes at 60 °C.

4% FLP 6, 70 °C. As described in the general method; 16.3 mg of FLP (0.04 mmol) was mixed with 61.9 mg (1.05 mmol) of $Me_2HN{\cdot}BH_3$ at 70 °C. NMR spectra were recorded after addition, 25, 40, 50, 95, 145, 175, 230, 3925, 4035, 5240, 6875 and 8145 minutes at 70 °C.

4% FLP 6, 80 °C. As described in the general method; 16.2 mg of FLP (0.04 mmol) was mixed with 61.5 mg (1.04 mmol) of $Me_2HN{\cdot}BH_3$ at 80 °C. NMR spectra were recorded after addition, 30, 55, 150, 180, 240 and 260 minutes at 80 °C.

1% FLP 6, 70 °C. As described in the general method; 4.2 mg of FLP (0.01 mmol) was mixed with 61.7 mg (1.05 mmol) of $Me_2HN{\cdot}BH_3$ at 70 °C. NMR spectra were recorded after addition, 35, 80, 140, 185, 350, 1450, 1745 minutes at 70 °C.

7.5% FLP 6, 70 °C. As described in the general method; 32.4 mg of FLP (0.08 mmol) was mixed with 62.8 mg (1.07 mmol) of $Me_2HN{\cdot}BH_3$ at 70 °C. NMR spectra were recorded after addition, 30, 50, 100, 125, 170 minutes at 70 °C.

10% FLP 6, 70 °C. As described in the general method; 44.6 mg of FLP (0.11 mmol) was mixed with 61.9 mg (1.05 mmol) of $Me_2HN{\cdot}BH_3$ at 70 °C. NMR spectra were recorded after addition, 30, 45, 60, 95, 115, 150, 190 minutes at 70 °C.

Table 2. Consumption of $Me_2NH{\cdot}BH_3$ in time by **6** as catalyst at 50 °C, 60 °C, 70 °C and 80 °C.

Reaction temperature (°C)	t (min)	MeAB (%)	Conversion (%)*	TOF (h^{-1})**
50	0	99.7	0.3	
	10	99.4	0.6	
	35	99.4	0.6	0.27
	85	97.7	2.3	0.43
	115	95.4	4.6	0.63
	175	92.3	7.7	0.69
	235	90.7	9.3	0.62
60	0	99.5	0.5	
	20	99	1	
	60	93.4	6.6	
	95	88.6	11.4	1.89
	160	82.9	17.1	1.68
	225	79	21	1.47
	240	78.1	21.9	1.44
	1470	43	57	0.61
	1525	41.5	58.5	0.60
	1575	40.5	59.5	0.60
	1620	39.5	60.5	0.59
70	0	100	0	
	25	96.5	3.5	
	40	93	7	
	50	91.6	8.4	2.65
	95	85.3	14.7	2.44
	145	78.4	21.6	2.35
	175	76.3	23.7	2.13
	230	70.4	29.6	2.03
	6905	14.7	85.3	0.19
	8295	9.65	90.35	0.17
80	0	100	0	
	30	91.7	8.3	4.36
	55	85.5	14.5	4.15
	150	68.9	31.1	3.27
	180	66.8	33.2	2.91
	240	61.5	38.5	2.53

*Minor amounts of other dehydrogenation products of $Me_2NH{\cdot}BH_3$ were observed by ^{11}B NMR spectroscopy, therefore the conversion of DMAB was calculated as the consumption of the substrate. **The TOF was calculated as ([dehydrogenation products] / $[FLP]_0$) / time (h).

Computational details:

All structures were optimized at the ωB97X−D level of theory,[31] using Gaussian 09, Revision D01. Geometry optimizations were performed using the 6-31G(d) and 6-311G(d,p) basis set,[32,33] and the nature of each stationary point was confirmed by frequency calculations.

Table 3. Energies for the optimized structures, for the barriers for dihydrogen abstraction and elimination, for the phosphonium-borate intermediate, and for the overall reaction.

	E:	Δ*E* (kcal/mol)	Δ*G* (kcal/mol)
$Me_2NH{\cdot}BH_3 \rightarrow Me_2N{=}BH_2 + H_2$		4.91	-9.88
***t*Bu$_2$PCH$_2$BPh$_2$**			
FLP	-1184.24842311		
TS H_2 abstraction	-1346.02159968	3.71	13.49
phosphonium-borate	-1185.42879072	-0.39	-2.12
TS H_2 elimination	-1185.38361602	27.96	23.27
Me$_2$PCH$_2$BPh$_2$			
FLP	-948.44127657		
TS H_2 abstraction	-1110.20871791	7.31	16.02
phosphonium-borate	-949.60953730	7.21	4.25
TS H2 elimination	-949.57187600	30.84	25.21
H$_2$PCH$_2$BPh$_2$			
FLP	-869.82017057		
TS H2 abstraction	-1031.56957210	18.63	27.94
phosphonium-borate	-870.96863296	19.63	17.59
TS H_2 elimination	-870.93890687	38.28	33.06
Cl$_2$PCH$_2$BPh$_2$			
FLP	-1789.03009514		
TS H_2 abstraction	-1950.76749497	26.16	36.11
phosphonium-borate	-1790.16647554	27.21	23.80
TS H_2 elimination	-1790.14044230	43.55	37.52
Ph$_2$PCH$_2$BPh$_2$			
FLP	-1331.77579550		
TS H_2 abstraction	-1493.53937264	9.73	19.25
phosphonium-borate	-1332.94072227	9.30	6.70
TS H_2 elimination	-1332.90304184	32.94	25.85

$(CF_3)_2PCH_2BPh_2$			
FLP	-1543.70835864		
TS H_2 abstraction	-1705.44619866	25.88	36.62
phosphonium-borate	-1544.84218486	28.81	25.76
TS H_2 elimination	-1544.81376060	46.65	40.34
$Mes_2PCH_2BPh_2$			
FLP	-1567.60557329		
TS H_2 abstraction	-1729.37397566	6.71	15.19
phosphonium-borate	-1568.77538903	6.23	2.70
TS H_2 elimination	-1568.73849346	29.38	22.12
***t*$Bu_2PCH_2BMes_2$**			
FLP	-1420.07103016		
TS H_2 abstraction	-1581.82986407	12.71	25.24
phosphonium-borate	-1421.25313770	-1.48	-2.27
TS H_2 elimination	-1421.20547470	28.43	24.94
***t*$Bu_2PCH_2B(Ph$*m*$-CF_3)_2$**			
FLP	-2532.05673548		
TS H_2 abstraction	-2693.84249909	-4.19	7.12
phosphonium-borate	-2533.25390861	-10.94	-11.30
TS H_2 elimination	-2533.20058581	22.52	19.39
***t*$Bu_2PCH_2B(ArF_5)_2$**			
FLP	-2176.26373626		
TS H_2 abstraction	-2338.05606247	-8.31	2.63
phosphonium-borate	-2177.47294661	-18.49	-20.24
TS H_2 elimination	-2177.41709280	16.56	10.86
***t*$Bu_2PCH_2Bt Bu_2$**			
FLP	-1036.70450770		
TS H_2 abstraction	-1198.46709092	10.36	21.22
phosphonium-borate	-1037.87965363	2.89	1.53
TS H_2 elimination	-1037.82854610	34.96	31.19
***t*$Bu_2PCH_2B(CH_3)_2$**			
FLP	-800.90652640		
TS H_2 abstraction	-962.67494970	6.69	18.42
phosphonium-borate	-802.07503798	7.05	5.56
TS H_2 elimination	-802.03943269	29.39	24.49
***t*$Bu_2PCH_2B(CF_3)_2$**			
FLP	-1396.17834099		

TS H_2 abstraction	-1557.99002484	-20.45	-10.28
phosphonium-borate	-1397.40728070	-30.87	-31.13
TS H2 elimination	-1397.34160104	10.34	6.15
***t*Bu$_2$PCH$_2$BH$_2$**			
FLP	-722.26609832		
TS H_2 abstraction	-884.05079175	-3.52	6.40
phosphonium-borate	-723.45307049	-4.54	-6.55
TS H_2 elimination	-723.41259401	20.86	15.21
***t*Bu$_2$PCH$_2$BCl$_2$**			
FLP	-1641.53653082		
TS H_2 abstraction	-1803.31507200	0.34	11.12
phosphonium-borate	-1642.73303293	-10.52	-12.48
TS H_2 elimination	-1642.67824450	23.86	18.05
Mes$_2$PCH$_2$B(Ph*m*-CF$_3$)$_2$			
FLP	-2915.42034786		
TS H_2 abstraction	-3077.20266145	-2.02	7.02
phosphonium-borate	-2916.60852526	-5.29	-6.66
TS H_2 elimination	-2916.56085573	24.62	18.38
Mes$_2$PCH$_2$B(ArF$_5$)$_2$			
FLP	-2559.62695886		
TS H_2 abstraction	-2721.40726789	-0.77	9.09
phosphonium-borate	-2560.82700887	-12.74	-13.53
TS H_2 elimination	-2560.77673120	18.81	13.18
Mes$_2$PCH$_2$B*t*Bu$_2$			
FLP	-1420.06013718		
TS H_2 abstraction	-1581.82610141	8.24	20.45
phosphonium-borate	-1421.22534748	9.12	5.92
TS H_2 elimination	-1421.19870062	25.84	19.14
Mes$_2$PCH$_2$B(CH$_3$)$_2$			
FLP	-1184.25838865		
TS H_2 abstraction	-1346.02643153	6.93	17.69
phosphonium-borate	-1185.41779827	12.76	8.21
TS H_2 elimination	-1185.39112375	29.50	24.37
Mes$_2$PCH$_2$B(CF$_3$)$_2$			
FLP	-1779.53148996		
TS H_2 abstraction	-1941.33838696	-17.45	-6.33
phosphonium-borate	-1780.75068153	-24.75	-26.85

TS H_2 elimination	-1780.69106389	12.66	6.55
$Mes_2PCH_2BH_2$			
FLP	-1105.61613735		
TS H_2 abstraction	-1267.40133026	-3.83	6.69
phosphonium-borate	-1106.79837980	-1.57	-3.81
TS H_2 elimination	-1106.76656003	18.40	13.81
$Mes_2PCH_2BCl_2$			
FLP	-2024.88659564		
TS H_2 abstraction	-2186.66679880	-0.70	11.04
phosphonium-borate	-2026.07727876	-6.86	-7.37
TS H_2 elimination	-2026.02779735	24.19	19.04
$Mes_2PCH_2BCy_2$			
FLP	-1574.88390659		
TS H_2 abstraction	-1736.65089523	7.59	20.59
phosphonium-borate	-1576.04925283	9.03	7.41
TS H_2 elimination	-1576.01793395	28.69	25.38
$Ph_2PCH_2BMes_2$			
FLP	-1567.60273120		
TS H_2 abstraction	-1729.36432587	10.98	24.81
phosphonium-borate	-1568.76562677	10.57	9.57
TS H_2 elimination	-1568.73301165	31.04	26.63
$Ph_2PCH_2BtBu_2$			
FLP	-1184.23251976		
TS H_2 abstraction	-1345.99955434	7.56	18.98
phosphonium-borate	-1185.39862800	8.56	6.77
TS H_2 elimination	-1185.36512808	29.58	24.47

X-ray crystal structure determination for 2, 3 and 6:

The single-crystal X-ray diffraction studies were carried out on a Bruker-Nonius KappaCCD diffractometer at 123(2) K using Mo-Kα radiation (λ = 0.71073 Å) (**2, 6**) or Bruker D8 Venture diffractometer with Photon100 detector at 123(2) K using Mo-Kα radiation (λ = 0.71073 Å) (**3**). Direct Methods (SHELXS-97)[34] were used for structure solution and refinement was carried out using SHELXL-2013/2014 (full-matrix least-squares on F^2).[35] Hydrogen atoms were localized by difference electron density determination and refined

using a riding model (H(B, N, P) free). Semi-empirical absorption corrections were applied. For **3** an extinction correction was applied.

2: colorless crystals, $C_{21}H_{32}BP \cdot 0.5(C_7H_8)$, M_r = 372.31, crystal size 0.50 x 0.30 x 0.20 mm, monoclinic, space group *C*2/*c* (no.15), *a* = 32.562(4) Å, *b* = 8.776(1) Å, *c* = 17.801(2) Å, β = 118.75(1)°, *V* = 4459.8(10) Å^3, *Z* = 8, ρ =1.109 Mg/m^{-3}, μ(Mo-K$_\alpha$) = 0.13 mm^{-1}, *F*(000) = 1624, $2\theta_{max}$ = 55°, 25741 reflections, of which 5128 were independent (R_{int} = 0.039), 243 parameters, R_1 = 0.049 (for 4179 I > 2σ(I)), wR_2 = 0.123 (all data), *S* = 1.03, largest diff. peak / hole = 0.88 / -0.44 e Å $^{-3}$.

3: colorless crystals, $C_{21}H_{34}B_2NP$, M_r = 353.08, crystal size 0.48 x 0.48 x 0.36 mm, triclinic, space group *P*-1 (no.2), *a* = 9.0523(5) Å, *b* = 10.2844(6) Å, *c* = 13.0205(8) Å, α = 100.971(2)°, β = 108.436(2)°, γ = 104.693(2)°, *V* = 1062.92(11) Å^3, *Z* = 2, ρ = 1.103 Mg/m^{-3}, μ(Mo-K$_\alpha$) = 0.13 mm^{-1}, *F*(000) = 384, $2\theta_{max}$ = 55°, 36356 reflections, of which 4902 were independent (R_{int} = 0.022), 239 parameters, R_1 = 0.032 (for 4554 I > 2σ(I)), wR_2 = 0.085 (all data), *S* = 1.05, largest diff. peak / hole = 0.35 / -0.28 e Å $^{-3}$.

6: orange crystals, $C_{27}H_{42}BP$, M_r = 408.38, crystal size 0.60 x 0.45 x 0.40 mm, monoclinic, space group $P2_1/c$ (no.14), *a* = 12.842(1) Å, *b* = 10.033(1) Å, *c* = 20.516(2) Å, β = 104.46(1)°, *V* = 2559.6(4) Å^3, *Z* = 4, ρ = 1.060 Mg/m^{-3}, μ(Mo-K$_\alpha$) = 0.12 mm^{-1}, *F*(000) = 896, $2\theta_{max}$ = 55°, 24882 reflections, of which 5871 were independent (R_{int} = 0.054), 268 parameters, R_1 = 0.050 (for 4666 I > 2σ(I)), wR_2 = 0.135 (all data), *S* = 1.05, largest diff. peak / hole = 0.40 / -0.35 e Å $^{-3}$.

2.5 References

[1] G. C. Welch, R. R. S. Juan, J. D. Masuda, D. W. Stephan, *Science*, **2006**, *314*, 1124–1126.

[2] For an overview of developments in FLP chemistry, see: a) D. W. Stephan, G. Erker, *Angew. Chem. Int. Ed.* **2010**, *49*, 46–76. b) D. W. Stephan, *Acc. Chem. Res.* **2015**, *48*, 306–316. c) D. W. Stephan, *Science* **2016**, *354*, 1248.

[3] C. W. Hamilton, R. T. Baker, A. Staubitz, I. Manners, *Chem. Soc. Rev.* **2009**, *38*, 279–293.

[4] a) T. B. Marder, *Angew. Chem. Int. Ed.* **2007**, *46*, 8116–8118. b) A. Staubitz, A. P. M. Robertson, M. E. Sloan, I. Manners, *Chem. Rev.* **2010**, *110*, 4023–4078. c) A. Staubitz, A. P. M. Robertson, I. Manners, *Chem. Rev.* **2010**, *110*, 4079–4124.

[5] E. M. Leitao, T. Jurca, I. Manners, *Nat. Chem.* **2013**, *5*, 817–829.

[6] For reviews about transition metal based amine-borane dehydrogenation catalysts, see: a) N. C. Smythe, J. C. Gordon, *Eur. J. Inorg. Chem.* **2010**, 509–521. b) N. E. Stubbs, A. P. M. Robertson, E. M. Leitao, I. Manners, *J. Organomet. Chem.* **2013**, *730*, 84–89. c) A. Rossin, M. Peruzzini, *Chem. Rev.* **2016**, *116*, 8848−8872. d) S. Bhunya, T. Malakar, G. Ganguly, A. Paul, *ACS Catal.* **2016**, *6*, 7907−7934.

[7] For reviews on group 1 and 2 metal based amine-borane dehydrogenation catalysts, see: a) R. J. Less, R. L. Melen, D. S. Wright, *RSC Adv.* **2012**, *2*, 2191–2199. b) R. L. Melen, *Chem. Soc. Rev.* **2016**, *45*, 775–788.

[8] a) D. W. Stephan, G. Erker, *Angew. Chem. Int. Ed.* **2010**, *49*, 46–76. b) D. W. Stephan, G. Erker, *Angew. Chem. Int. Ed.* **2015**, *54*, 6400–6441.

[9] C. Appelt, J. C. Slootweg, K. Lammertsma, W. Uhl, *Angew. Chem. Int. Ed.* **2013**, *52*, 4256–4259.

[10] M. W. Lui, N. R. Paisley, R. McDonald, M. J. Ferguson, E. Rivard, *Chem. Eur. J.* **2016**, *22*, 2134– 2145.

[11] Z. Mo, A. Rit, J. Campos, E. L. Kolychev, S. Aldridge, *J. Am. Chem. Soc.* **2016**, *138*, 3306−3309.

[12] J. Possart, W. Uhl, *Organometallics*, **2018**, *37*, 1314−1323.

[13] M. Boudjelel, E. D. S. Carrizo, S. Mallet−Ladeira, S. Massou, K. Miqueu, G. Bouhadir, D. Bourissou, *ACS Catal.* **2018**, *8*, 4459−4464.

[14] Reactivity towards small molecules: a) F. Bertini, V. Lyaskovskyy, B. J. J. Timmer, F. J. J. de Kanter, M. Lutz, A. W. Ehlers, J. C. Slootweg, K. Lammertsma, *J. Am. Chem. Soc.* **2012**, *134*, 201−204. b) E. R. M. Habraken, L. C. Mens, M. Nieger, M. Lutz, A. W. Ehlers, J. C. Slootweg, *Dalton Trans.* **2017**, *46*, 12284−12292

[15] Reactivity towards transition metals: a) D. H. A. Boom, A. W. Ehlers, M. Nieger, J. C. Slootweg, *Z. Naturforsch., B: Chem. Sci.* **2017**, *72*, 781−784. b) D. H. A. Boom, A. W. Ehlers, M. Nieger, M. Devillard, G. Bouhadir, D Bourissou, J. C. Slootweg, *ACS Omega*, **2018**, *3*, 3945–3951.

[16] See Experimental Details.

[17] For examples of cyclic phosphine-boranes see: H. Schmidbaur, M. Sigl, A. Schier, *J. Organomet. Chem.* **1997**, *529*, 323–327.

[18] a) A. P. M. Robertson, E.M. Leitao, I. Manners, *J. Am. Chem. Soc.* **2011**, *133*, 19322–19325. b) E. M. Leitao, N. E. Stubbs, A. P. M. Robertson, H. Helten, R. J. Cox, G. C. Lloyd-Jones, I. Manners, *J. Am. Chem. Soc.* **2012**, *134*, 16805−16816.

[19] a) N. M. D. Brown, F. Davidson, J. W. Wilson, *J. Organomet. Chem.* **1980**, *192*, 133−138. b) R. A. Bartlett, H. Chen, V. R. Dias, M. M. Olmstead, P. P. Power, *J. Am. Chem. Soc.* **1988**, *110*, 446−449.

[20] In addition, 2-MeTHF is less prone ring opening polymerization: E. Piedra-Arroni, C. Ladavière, A. Amgoune, D. Bourissou, *J. Am. Chem. Soc.* **2013**, *135*, 13306−13309.

[21] D. García-Vivó, E, Huergo, M. A. Ruiz, R. Travieso-Puente, *Eur. J. Inorg. Chem.* **2013**, 4998−5008.

[22] For examples of catalyst design in FLP chemistry see: a) L. Zhao, G. Lu, F. Huang, Z.-X. Wang, *Dalton Trans.* **2012**, *41*, 4674–4684. b) M. V. Mane, M. A. Rizvi, K. Vank, *J. Org. Chem.* **2015**, *80*, 2081−2091. c) L. Liu, N. Vankova, T. Heine, *Phys. Chem. Chem. Phys.* **2016**, *18*, 3567−3574. d) G. Ma, Z. H. Li, *Phys.*

Chem. Chem. Phys. **2016**, *18*, 11539−11549. e) F.-G. Fontaine, M.-A. Courtemanche, M.-A. Légaré, É. Rochette, *Coord. Chem. Rev.* **2017**, *334*, 124−135. f) M. V. Mane, K. Vanka, *ChemCatChem*, **2017**, *9*, 3013−3022.

[23] For an example of rational catalyst design for amine-borane dehydrogenation by FLPs see: a) Y. Guo, X. He, Z. Li, Z. Zou, *Inorg. Chem.* **2010**, *49*, 3419–3423. b) G. Ma, G. Song, Z. H. Li, *Chem. Eur. J.* 10.1002/chem.201801932.

[24] For Csp^2–H activation see: a) M. -A. Légaré, M.-A. Courtemanche, É. Rochette, F.-G. Fontaine, *Science* **2015**, *349*, 513−516. b) M.-A. Légaré, E. Rochette, J. L. Lavergne, N. Bouchard, F.-G. Fontaine, *Chem. Commun.* **2016**, *52*, 5387−5390. c) J. L. Lavergne, A. Jayaraman, L. C. M. Castro, É. Rochette, F.-G. Fontaine, *J. Am. Chem. Soc.* **2017**, *139*, 14714−14723. For Csp^3–H activation see: d) É. Rochette, M.-A. Courtemanche, F.-G. Fontaine, *Chem. Eur. J.* **2017**, *23*, 3567–3571. For C−S activation see: e) É. Rochette, H. Boutin, F.-G. Fontaine, *Organometallics* **2017**, *36*, 2870−2876.

[25] For an overview on the reactivity of *ortho*-phenylene bridged amine-borane FLPs see: F.-G. Fontaine, É. Rochette, *Acc. Chem. Res.* **2018**, *51*, 454−464.

[26] C. D. Roy, R. Soundararajan, H. C. Brown, *Monatsh. Chem.* **2008**, *139*, 241–249.

[27] a) T. Kawashima, T. Kannabe, N. Tokitoh, R. Okazaki, *Organometallics* **1999**, *18*, 5180–5182. b) F. Lavigne, E. Maerten, G. Alcaraz, N. Saffon-Merceron, C. Acosta-Silva, V. Branchadell, A. Baceiredo, *J. Am. Chem. Soc.* **2010**, *132*, 8864–8865.

[28] F. Eisenträger, A. Göthlich, I. Gruber, H. Heiss, C. A. Kiener, C. Krüger, J. U. Notheis, F. Rominger, G. Scherhag, M. Schultz, B. F. Straub, M. A. O. Volland, P. Hofmann, *New. J. Chem.* **2003**, *27*, 540−550.

[29] N. M. D. Brown, F. Davidson, R. McMullan, J. W. Wilson, *J. Organomet. Chem.* **1980**, *193*, 271−282.

[30] A. Sundararaman, F. Jäkle, *J. Organomet. Chem.* **2003**, *681*, 134−142.

[31] J.-D. Chai, M. Head-Gordon, M. *Phys. Chem. Chem. Phys.* **2008**, *10*, 6615–6620.

[32] a) R. Ditchfield, W. J. Hehre, J. A. Pople, *J. Chem. Phys.* **1971**, *54*, 724–728. b) W. J. Hehre, R. Ditchfield, J. A. Pople, *J. Chem. Phys.* **1972**, *56*, 2257–2261. c) P. C. Hariharan, J. A. Pople, *Theor. Chem. Acc.* **1973**, *28*, 213–222. d) P. C. Hariharan, J. A. Pople, *Mol. Phys.* **1974**, 27, 209–214. e) M. S. Gordon, *Chem. Phys. Lett.* **1980**, *76*, 163–168. f) M. M. Francl, W. J. Pietro, W. J. Hehre, J. S. Binkley, D. J. DeFrees, J. A. Pople, M. S. Gordon, *J. Chem. Phys.* **1982**, *77*, 3654–3665. g) R. C. Binning, Jr., L. A. Curtiss, *J. Comp. Chem.* **1990**, *11*, 1206–1216. h) J.-P. Blaudeau, M. P. McGrath, L. A. Curtiss, L. Radom, *J. Chem. Phys.* **1997**, *107*, 5016–5021. i) V. A. Rassolov, J. A. Pople, M. A. Ratner, T. L. Windus, *J. Chem. Phys.* **1998**, *109*, 1223–1229. j) V. A. Rassolov, M. A. Ratner, J. A. Pople, P. C. Redfern, L. A. Curtiss, *J. Comp. Chem.* **2001**, *22*, 976–984.

[33] For the polarization functions, see: M. J. Frisch, J. A. Pople, J. S. Binkley, *J. Chem. Phys.* **1984**, *80*, 3265–3269.

[34] G. M. Sheldrick, *Acta Crystallogr.* **2008**, *A64*, 112–122.

[35] G. M. Sheldrick, *Acta Crystallogr.* **2015**, *C71*, 3–8.